Soil respiration phenology improves modeled phase of terrestrial net ecosystem exchange in northern hemisphere

K. Arthur Endsley[1], John S. Kimball[1], Rolf H. Reichle[2]

[1]Numerical Terradynamic Simulation Group (NTSG), W.A. Franke College of Forestry and Conservation, University of Montana, Missoula, MT
[2]Global Modeling and Assimilation Office, NASA Goddard Space Flight Center, Greenbelt, Maryland, USA

Key Points:

- A bias in the seasonal cycle of net ecosystem exchange at high northern latitudes is identified in a first-order soil decomposition model
- Soil respiration processes that reduce or delay respiration during spring mitigate this phase bias and improve modeling skill
- In situ chamber measurements of soil respiration provide validation and verification of model enhancements

Corresponding author: K. Arthur Endsley, `arthur.endsley@ntsg.umt.edu`

Abstract

In the northern hemisphere, terrestrial ecosystems transition from net sources of CO2 to the atmosphere in winter to net ecosystem carbon sinks during spring. The timing (or phase) of this transition, determined by the balance between ecosystem respiration (RECO) and primary production, is key to estimating the amplitude of the terrestrial carbon sink. We diagnose an apparent phase bias in the RECO and net ecosystem exchange (NEE) seasonal cycles estimated by the Terrestrial Carbon Flux (TCF) model framework and investigate its link to soil respiration mechanisms. Satellite observations of vegetation canopy conditions, surface meteorology, and soil moisture from the NASA SMAP Level 4 Soil Moisture product are used to model a daily carbon budget for a global network of eddy covariance flux towers. Proposed modifications to TCF include: the inhibition of foliar respiration in the light (the Kok effect); a seasonally varying litterfall phenology; an O2 diffusion limitation on heterotrophic respiration (RH); and a vertically resolved soil decomposition model. We find that RECO phase bias can result from bias in RECO magnitude and that mechanisms which reduce northern spring RECO, like substrate and O2 diffusion limitations, can mitigate the phase bias. A vertically resolved soil decomposition model mitigates this bias by temporally segmenting and lagging RH throughout the growing season. Applying these model enhancements at Continuous Soil Respiration (COSORE) sites verifies their improvement of RECO and NEE skill compared to in situ observations (up to $\Delta\text{RMSE} = -0.76\, g\, C\, m^{-2}\, d^{-1}$). Ultimately, these mechanisms can improve prior estimates of NEE for atmospheric inversion studies.

Plain Language Summary

In the northern hemisphere, the plants and the soil respond to warming temperatures and increasing day lengths in spring and begin to store more carbon than they release to the atmosphere, on average. The timing of this change is very important for accurately modeling how much carbon is stored or released to the atmosphere. We found that a commonly used model of plants and soil has delayed predictions of the timing of this seasonal cycle of carbon. We studied different potential changes to the model, including changes to: how carbon inputs to the soil from plant roots, dead leaves, and down wood are added over time; how soil microbes respond to high levels of soil moisture; whether the soil is represented by a single layer or by multiple layers at different depths; and how the release of carbon by plants varies with solar radiation. We found that multiple different changes resulted in similar corrections to the seasonal cycle of carbon so long as they reduced or delayed the amount of carbon released during the spring season. We discuss why that is and how it impacts the model's performance and its importance for other modeling studies.

1 Introduction

In northern hemisphere temperate, boreal, and tundra regions, the spring season is marked by an increase in temperature and day length, stimulating vegetation photosynthesis and growth. A result of this increased primary production is that northern ecosystems transition from net sources of CO_2 to the atmosphere during the winter to net ecosystem carbon sinks during spring. The timing of this transition is determined by the balance between ecosystem respiration (RECO) and primary production (Chapin et al., 2006; Noormets et al., 2009). The northern land sink dominates the global, terrestrial carbon sink and its seasonal amplitude has been increasing for decades (Graven et al., 2013; Forkel et al., 2016; Ciais et al., 2019).

At high northern latitudes ($\geq 40N$) where there is strong seasonal variation in conditions that support soil decomposition and plant growth, the timing of soil respiration phenology is key to accurately estimating the amplitude of the terrestrial carbon sink (Zhao & Zeng, 2014; Migliavacca et al., 2015; Parazoo et al., 2018). Changes in the on-

set of the growing season, such as an earlier start of spring or delayed start of autumn, may lead to a longer carbon uptake period (Wu et al., 2013; Keenan et al., 2014) provided that concurrent increases in RECO are smaller (Richardson et al., 2010); i.e., that the carbon flux to plants and the soil is larger than the respired CO_2 flux to the atmosphere. Thus, the northern hemisphere (NH) seasonal cycle of carbon uptake is an emergent property (Birch et al., 2021) that depends upon the timing and relative magnitudes of multiple component ecosystem sources and sinks. Shifts in the modeled seasonal carbon uptake period, relative to atmospheric inversion data or multi-model means, can be substantial and generally point to significant model biases (Forkel et al., 2014; Ito et al., 2016; Zhao et al., 2016).

Models are, necessarily, simplified representations of complex ecosystem processes and direct observation of some CO_2 fluxes is infeasible at large scales (Bond-Lamberty et al., 2016). However, satellite observations of vegetation provide a strong constraint on canopy phenology and on net (NPP) and gross primary productivity (GPP). In northern ecosystems, they are also a strong constraint on net ecosystem CO_2 exchange (NEE) due to the tight link between plant productivity and the seasonal increase in CO_2 uptake (Järveoja et al., 2018). Models without direct observations of canopy conditions tend to have biases in simulated GPP that propagate to other modeled fluxes (e.g., Thum et al., 2020). The ability to directly observe canopy changes has previously been used to diagnose model biases in northern ecosystem GPP (Peng et al., 2015; Shi et al., 2020; Birch et al., 2021).

Here, we diagnose an apparent bias in the NH seasonal cycle of RECO in the Terrestrial Carbon Flux (TCF) model framework (Kimball et al., 2009), which combines a satellite data-driven light-use efficiency (LUE) model with a first-order soil decomposition model to estimate a daily carbon budget. The TCF framework has been used to infer climate impacts on northern ecosystems' productivity and soil carbon (Yi et al., 2013; Watts et al., 2014) and is part of the NASA Soil Moisture Active Passive (SMAP) mission Level 4 Carbon (L4C) operational product (Entekhabi et al., 2010; Jones et al., 2017; Endsley et al., 2020). A bias in the timing of the RECO seasonal cycle or its components, heterotrophic respiration (R_H) and autotrophic respiration (R_A), can result in a bias in the seasonal cycle of NEE (Noormets et al., 2009; Alexandrov, 2014) and limits the use of data-driven terrestrial carbon flux estimates as priors in atmospheric inversion studies (Byrne et al., 2018). Identifying and mitigating such biases can generate insight into the biotic and abiotic factors that influence CO_2 exchange between the land and atmosphere, informing future model developments. Whereas previous studies of potential biases in carbon flux estimates have tended to focus on GPP (e.g., Zhao & Zeng, 2014; Migliavacca et al., 2015; Parazoo et al., 2018), here, we examine the role of model processes for estimating RECO.

Compared to eddy covariance (EC) flux tower and atmospheric inversion datasets, the timing of the seasonal change in NEE as modeled by TCF is delayed (Figure 1), likely as a result of an advanced RECO cycle. The temporal advance in the modeled RECO seasonal cycle suggests that canopy respiration or soil respiration are high-biased early in the growing season (NH spring). We also note that the NH summer NEE amplitude is under-estimated in TCF. This bias is common among terrestrial biosphere models (Peng et al., 2014). A similar NEE phase difference can be seen between the Carnegie-Ames Stanford Approach (CASA) and Simple Biosphere 3 (SiB3) models (Byrne et al., 2018). Our study aims to diagnose this issue and answer the broader questions:

1. Does a seasonally varying adjustment of RECO or its components, R_H and R_A, improve the fit in modeled NEE phase compared to observed NH ecosystem CO_2 fluxes from a global network of EC flux towers? This adjustment might take the form of either an explicit phenology model or a seasonally varying climatic response.

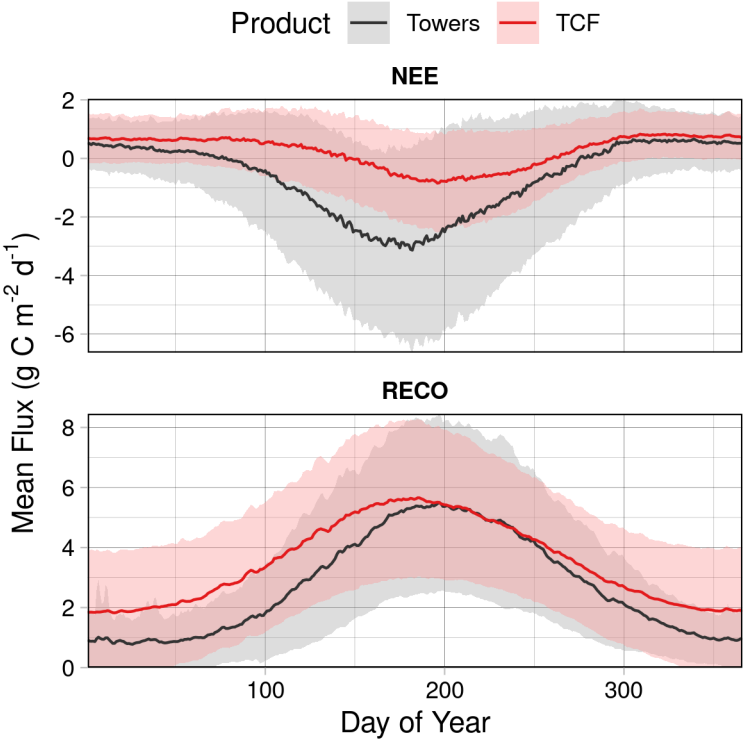

Figure 1. NEE and RECO mean seasonal cycles, as measured by EC flux towers ("Towers") or modeled by TCF, for tower sites north of 40 degrees N latitude. Shaded area represents one spatial standard deviation. TCF data are from the L4C Nature Run v8.3 simulation.

2. What is the impact of alternative R_H or R_A models on the mean RECO phase and estimation skill, validated against flux data measured at towers and *in situ* chamber sites?

We identified potential improvements to the TCF model based on mechanisms hypothesized to affect the timing of RECO components that are missing or inadequately represented in the current framework. Potential improvements should be consistent with an operational, data-driven, and low-latency daily model such as SMAP L4C. We did not consider refinements to the LUE model or GPP parameters in this study because GPP in TCF is constrained by satellite-observed vegetation phenology.

Specifically, we hypothesized that one or a combination of processes might be critical to the correct timing of the RECO seasonal cycle in the NH: seasonally varying litterfall inputs to SOC, which would enhance an R_H phenology; an upper limit on the response of R_H to soil moisture (SM) due to limited O_2 diffusion at near-saturating SM conditions, which may occur seasonally; and the slow diffusion of heat and moisture across vertically stratified soil layers, which can result in temporally lagged R_H flux. The RECO seasonal cycle could also be adjusted by changes to the R_A component; for example, through modeling of the inhibition of leaf R_A in the light (Wehr et al., 2016; Keenan et al., 2019), also known as the Kok effect, which could reduce the high RECO bias during the NH spring (Heskel et al., 2013; Byrne et al., 2018), as the TCF framework lumps above- and below-ground R_A together. Other potential modifications to the R_A model not investigated here include increased construction respiration during spring leaf-out (Papale &

Valentini, 2003) or increased respiration associated with the maintenance of photosynthetic rates (Migliavacca et al., 2015)

These hypotheses have support in the literature. The Kok effect is well-known, despite uncertainty regarding the cellular mechanism(s) responsible (Heskel et al., 2013). A seasonally varying litterfall scheme is intuitive and consistent with observations of soil respiration in the NH fall season (Davidson et al., 2006) and experimental manipulations of litter inputs (Leitner et al., 2016; Nielsen et al., 2019). A looser coupling of litterfall and GPP is also consistent with the finding that peak below- and above-ground respiration are temporally separated (Davidson et al., 2006; Giasson et al., 2013). An O_2 diffusion limitation has been implemented in other terrestrial carbon flux models (Davidson et al., 2012; Sihi et al., 2018) and has some experimental support. For instance, Järveoja et al. found that the temperature sensitivity of R_H in northern peatlands is enhanced in dry periods, possibly due to increased O_2 supply to heterotrophs. It has also been found to improve RECO estimation at wetland sites (Sulman et al., 2012) and where snowmelt also leads to an increase in soil water content in spring (Oikawa et al., 2014; Winnick et al., 2020). A vertically stratified soil column has been adopted in land models (Tao et al., 2017; dos Santos et al., 2021). The mechanics of heat diffusion suggest that surface layers of the soil will warm before deeper layers, inducing lagged respiration throughout the soil column. This time lag, most evident in the spring and fall, has been associated with changes in the share of ecosystem respiration from the soil (Davidson et al., 2006). Vertical variation in soil temperature, in particular, has been shown to substantially improve soil carbon stock estimates at high latitudes (Koven et al., 2017; Yi et al., 2020).

2 Data and Methods

We modified the open-source TCF source code (Endsley, 2021a) to support the respiration processes hypothesized to affect the timing of the NEE and RECO seasonal cycles. In TCF, soil decomposition proceeds according to first-order kinetics as a function of litterfall inputs and the total SOC substrate (Jones et al., 2017; Endsley et al., 2020). The base rates of decomposition, or (inverse) turnover times, are modified by environmental constraint functions. Surface SM is used to model the response of R_H to substrate availability; i.e., liquid water in the soil pore spaces allows microbes to access organic carbon substrates, the decomposition of which produces a CO_2 flux (R_H). Soil temperature in the top 5 cm also promotes soil decomposition, modeled by an Arrhenius temperature function. Daily litterfall is computed as a constant daily fraction of annual NPP.

The response of R_H to surface SM and temperature is calibrated against a representative, global set of EC flux towers, separately, for towers representing different Plant Functional Types (PFTs), using constrained non-linear least squares optimization. The global distribution of up to eight PFT classes are defined from the MODIS MOD12Q1 (Type 5) land-cover classification (Friedl et al., 2010): Evergreen Needleleaf Forest (ENF), Evergreen Broadleaf Forest (EBF), Deciduous Needleleaf Forest (DNF), Deciduous Broadleaf Forest (DBF), Shrubland (SHB), Grassland (GRS), Cereal Crop (CCR), and Broadleaf Crop (BCR).

In this study, the L4C Nature Run version 8.3 (NRv8.3), a model-only version of L4C uninformed by SMAP satellite brightness temperatures, is used as the baseline version of TCF against which potential model enhancements are evaluated. L4C NRv8.3 is, in turn, based on soil moisture and temperature data from the SMAP Level 4 Soil Moisture (L4SM) Nature Run version 8.3, a model-only version of the operational SMAP L4SM product (Reichle et al., 2019, 2017). Both the operational SMAP L4C Version 5 and L4C NRv8.3 have the same model logic, with NEE computed as the residual difference between GPP and RECO. L4C NRv8.3 and the modified versions of TCF use the same daily surface meteorological driver data for the period January 1, 2000 through December 31,

2017. For each modification to TCF, a full, daily carbon budget was calculated at 356 EC flux tower sites from the FLUXNET La Thuille Collection (Baldocchi, 2008). The modeled fluxes are site-scale, representing a 9-km area centered on each EC tower site; model processing occurs at 1-km spatial resolution within that footprint.

The GPP model of L4C NRv8.3 is unchanged throughout this study; each experiment uses the same minimum air temperature, vapor pressure deficit (VPD), and photosynthetically active radiation (PAR) data from the Modern Era Retrospective Re-analysis (MERRA-2, Gelaro et al., 2017). Similarly, the fraction of PAR absorbed by the canopy (fPAR) is derived from the Moderate Resolution Imaging Spectroradiometer (MODIS) MCD15A2H product (Myneni et al., 2015) and is used as a model input to compute identical GPP estimates in each experiment. The environmental responses for each PFT in L4C NRv8.3 and subsequent experiments were calibrated against observed GPP and RECO fluxes partitioned from daily NEE using the night-time method at representative tower sites (Keenan et al., 2019). In every experiment, the three SOC pools (stratified by base decomposition rates) were brought to steady-state conditions through an analytical spin-up followed by a numerical spin-up, consisting of repeated cycling of annual climatologies until the annual NEE balance is within $\pm 1\, g\, C\, m^{-2}\, d^{-1}$.

2.1 Litterfall Phenology

The timing of litterfall allocation to SOC pools could have a profound effect on the seasonal cycle of R_H. Randerson et al. tested litterfall allocation schemes based on remotely sensed leaf-area index (LAI) and selected the best-performing scheme for the CASA model. The CASA litterfall scheme, as implemented in the modified TCF framework, changes litterfall input, $\mathcal{L}$, from a constant daily fraction of NPP to a moving-window function of LAI:

$$\mathcal{L}(t) = \text{NPP} \times (f_E\, \delta t + f_L(t)) \quad \text{where} \quad f_E = \frac{\min(\text{LAI})}{\text{mean}(\text{LAI})},\ t \in [1, 365] \tag{1}$$

Where t is the day-of-year; δt is the time step in years (1/365); f_E is the evergreen fraction, an estimate of the proportion of the canopy that is evergreen; and f_L is the litterfall fraction in excess of a constant daily fraction (1/365):

$$f_L(t) = \frac{L_{loss}(t)}{\sum L_{loss}(t)}(1 - f_E) \tag{2}$$

f_L is normalized by the annual sum of L_{loss}, the leaf-loss function. L_{loss} is a triangular moving window centered on the current time step, amounting to the difference between lagged and leading LAI. Here, satellite-observed LAI inputs to the TCF model are obtained from the MODIS MCD15A2H product (Myneni et al., 2015). Unlike Randerson et al., we re-calculate f_E each year, allowing for potential changes in the canopy species composition. We also used the full MODIS MCD15A2H record, down-scaled to daily time steps by forward-filling values, over the 2000-2017 period. The approach requires two leading values from MCD15A2H (two 8-day MCD15A2H composites), which would introduce a ca. 16-day latency. For an operational algorithm aiming for low latency, like SMAP L4C, a static 365-day LAI climatology could be used instead.

2.2 O_2 Diffusion Limitation

If O_2 diffusion becomes limiting at high SM, this could explain the apparent RECO high bias in TCF during the spring season. We verified that high SM conditions exist in the NH spring at multiple U.S. Surface Climate Observing Reference Networks (USCRN) (Diamond et al., 2013) and Soil Climate Analysis Network (SCAN) (Schaefer et al., 2007) *in situ* monitoring sites in the contiguous United States (CONUS) north of 40 degrees

latitude. An annual SM climatology, compiled for each sensor depth, based on these sites suggests that shallow soil layers, in particular, experience an increase in SM anomaly during the NH spring (Figure S1).

To model an O_2 diffusion limit at high SM conditions, we adopted a Michaelis-Menten (MM) function of soil volumetric water content (Davidson et al., 2012) as an additional constraint on R_H. Currently in TCF (NRv8.3), R_H from pool i is a function of the base decomposition, k_i, the amount of SOC, C_i, an Arrhenius function of soil temperature, $f(T)$, and a linear ramp function of soil wetness (volumetric percent of pore space occupied by liquid water), $g(\theta_{\%})$, representing substrate diffusion. In the modified TCF R_H function, $g(\theta_{\%})$ is replaced by the minimum of itself and the O_2 diffusion limit term, a function of the volumetric O_2 concentration, $[O_2]$, and the MM or half-saturation constant, $k_{M_{O_2}}$:

$$R_H = \sum_{i=1}^{3} k_i \times C_i \times f(T) \times \min\left(g(\theta_{\%}),\ \frac{[O_2]}{k_{M_{O_2}} + [O_2]}\right) \tag{3}$$

In taking the minimum of these two constraints, we assume they are equally limiting for soil heterotrophs. We calculate the O_2 concentration based on the diffusion coefficient of O_2 in the air, d_{gas}, the air fraction of O_2 ($0.209\ L\,L^{-1}$), the porosity of the soil, ϕ, and the volumetric soil moisture, θ. In our approach, no new fit parameters are required, as the constants $k_{M_{O_2}}$ and d_{gas} can be identified based on the soil moisture distribution observed among sites with the same PFT. First, following Davidson et al., we assume that when soil moisture is very low (below 5th percentile), the O_2 concentration in the soil pore spaces is the same as in the air, leading to:

$$[\mathrm{O_2}] = 0.209\, d_{gas}(\phi - \theta)^{4/3} \quad \longrightarrow \quad d_{gas} = \lim_{\theta \to 0}(\phi - \theta)^{-4/3} \tag{4}$$

Second, we set $k_{M_{O_2}} \equiv [O_2]$, calculated using this inferred value of d_{gas} and the median soil moisture. As in NRv8.3, soil moisture and porosity are derived from the SMAP L4SM (Reichle et al., 2019) and GEOS-5 Catchment Land Model (Koster et al., 2000; Tao et al., 2017), respectively.

2.3 Vertically Resolved Soil Decomposition Model

The original TCF framework is not vertically stratified: soil decomposition and R_H flux are considered to occur near the surface in a single soil layer of arbitrary thickness. The SMAP L4SM product estimates soil temperatures in seven layers with interfaces at 5, 15, 35, 75, 150, and 300 cm depth, accounting for bedrock. However, because of the particular structure of the Catchment model, L4SM only reports SM in three nested layers: the surface layer (0-5 cm), the root-zone (approximately 0-100 cm), and the soil profile (0 cm to bedrock depth). In order to obtain vertically resolved estimates of soil water content, we developed a simple physical model of soil water infiltration, diffusion, and lateral drainage (Endsley, 2021b) based on the modified Richards' equation and which is fully described in Appendix A. The corresponding, vertically stratified soil decomposition model is driven with these estimates of the soil water profile, which depend on surface infiltration estimates from L4SM, while L4C NRv8.3 is driven using L4SM surface soil moisture.

The multi-layer soil profile modification to TCF includes modifications of the SOC and R_H sub-models. The new, vertically resolved SOC model is similar to that of Yi et al.:

$$\frac{\partial}{\partial t}C_i(z) = \mathcal{R}_i(z) - k_i C_i(z) + \frac{\partial}{\partial z}\left(D(z)\frac{\partial C_i}{\partial z}\right) \tag{5}$$

Where $\mathcal{R}_i(z)$ represents inputs (and transfers) to SOC pool i at depth z and $D(z)$ is the vertical diffusivity of SOC. Diffusivity is taken to be $2 \times 10^{-4}\, m^2\, yr^{-1}$, after Yi

et al. for non-permafrost soils. Each soil layer or depth, z, contains the same three SOC pools, which are the same pools in the baseline NRv8.3 and the other experiments. Litterfall input is now a function of depth:

$$\mathcal{R}_i(z) = \mathcal{L}_i(z) + f_{ji} \quad \text{where} \quad \mathcal{L}_i(z) = \mathcal{L}_i \times \exp\left(-\frac{z}{z_e}\right) \tag{6}$$

Where $\mathcal{L}_i(z)$ is the litterfall input to SOC pool i at depth z, an exponentially declining function of depth, after Koven et al., which estimated the e-folding depth, z_e, to be equal to 10 cm. $\mathcal{L}_i$, the total daily litterfall input across the soil profile, is estimated as in NRv8.3 as a constant daily fraction of NPP. f_{ji} is the transfer function defining carbon (C) transfers from pool j to pool i.

Finally, R_H is calculated similar to the baseline TCF model, NRv8.3, with environmental modifiers soil moisture and temperature, but as a composite sum of the R_H in each soil layer and with an additional rate modifier, $h(z)$, which accounts for the extinction of R_H with depth due to factors *other than* soil moisture or temperature (Koven et al., 2013):

$$R_H = \sum_{z=1}^{Z} \sum_{i=1}^{3} k_i \, C_{i,z} \, f(T_z) \, g(\theta_z) \, h(z) \quad \text{where} \quad h(z) = \exp\left(-\frac{z}{z_k}\right) \tag{7}$$

z_k, the depth at which environmentally-constrained R_H declines by a factor of e (due to, e.g., mineral protection, aggregation, etc.), is a free parameter that is fit in calibration against the observed RECO flux.

2.4 The Kok Effect

To simulate the inhibition of R_A by light (the Kok effect), prior modeling studies have modulated maximum light-use efficiency (LUE) according to irradiance (Turner et al., 2006) or adjusted R_A directly as a function of irradiance, solar elevation, and the leaf angle distribution (Wohlfahrt et al., 2005). In TCF, however, a potential inhibition of R_A implicates both the calibration and forward modeling through plant carbon use efficiency (CUE), or the fraction of GPP that is not respired. During calibration, CUE is used to compute R_H for fitting against EC flux tower observations. In this experiment, CUE now varies with PAR:

$$R_H = \text{RECO} - R_A \tag{8}$$
$$= \text{RECO} - (1 - CUE \times g(PAR)) \times \text{GPP} \tag{9}$$

Where $g(PAR)$ is a linear ramp function that monotonically increases with increasing PAR:

$$g(x) = \begin{cases} 1 & \text{if } x \geq x_{max} \\ 0 & \text{if } x \leq x_{min} \\ \frac{x - x_{min}}{x_{max} - x_{min}} & \text{otherwise} \end{cases} \tag{10}$$

Where x_{min} and x_{max} are the lower and upper bounds of the ramp function. In the experiment NRv8.3 + Kok Effect, x_{min} and x_{max} are fit parameters. In the baseline TCF NRv8.3, CUE does not vary with PAR (i.e., $g(PAR) \equiv 1$).

During forward modeling, CUE is key to computing NEE as the residual between RECO and GPP or, equivalently, between R_H and NPP:

$$\text{NEE} = R_H - \text{NPP} \tag{11}$$
$$= R_H - [CUE \times g(PAR) \times \text{GPP}] \tag{12}$$

2.5 Verification and Validation against Flux Tower Observations

The mean seasonal cycle at the 356 EC tower sites was used as a within-sample check on the experimental results, as it is observed that the mean seasonal cycle of the calibrated model does not match that of the underlying calibration data for high northern latitudes (Figure 1); i.e., does the modified TCF model display better fidelity to NH seasonal cycles in the calibration dataset? In addition to this model verification, we validated RECO and NEE modeling skill, in carbon terms, against the L4C Core Validation Sites (CVS) (Jones et al., 2017).

We also validated the TCF mean seasonal cycles against that of the FLUXCOM up-scaled tower fluxes dataset (Jung et al., 2020), which is based on the random forest method with combined remote sensing and meteorology drivers (RS+METEO). Like FLUXCOM, TCF-based models (e.g., SMAP L4C) extrapolate to the global land domain the site-level relationships between environmental drivers and carbon fluxes, based on a representative set of EC flux towers. Though not entirely independent of the FLUXNET towers used to calibrate TCF, the additional driver datasets and larger spatial extent of FLUXCOM motivate our comparison of the aggregate, mean NEE and RECO seasonal cycles. Unlike the EC tower data, FLUXCOM provides gridded data over land; we subset the data to all pixels $\geq$ 40 N latitude. As the global network of 356 EC towers used to calibrate TCF are assumed to be sufficiently representative for inferring relationships at global scale, we compared the aggregated mean seasonal cycle from FLUXCOM's larger spatial extent to that of our site-level modeled results.

Two techniques were used to quantify the effect of each TCF modification on the modeled NEE and RECO seasonal cycles. First, we applied a low-pass filter (smoother) to the mean seasonal cycle, aggregated across all towers matching each PFT or across the FLUXCOM time series. We chose a 7-day moving window for the filter based on visual inspection of the filtered results. Second, we used Fourier regression to quantify the phase shift, in days, of a harmonic function fit to the FLUXCOM time series or the complete time series of all tower sites within each PFT group. Specifically, with smoothing, we aggregated the mean seasonal cycle prior to applying the filter; with Fourier regression, the raw time series data were used to estimate model parameters. Fourier regression provides a standard error for the phase offset across PFTs; the low-pass filter provides an estimate of the location of minimum NEE or maximum RECO.

2.6 Validation against Chamber Data

We used data from the Community Soil Respiration (COSORE) database (Bond-Lamberty et al., 2020), a collection of *in situ* chamber studies, to investigate the relative advantage of each TCF modification and validate the modeled RECO fluxes. As TCF does not distinguish between above-ground and below-ground respiration and calculates R_A as a constant fraction of GPP, we assume that TCF RECO is roughly proportional to soil respiration (R_S) at daily time scales. R_S should be the largest component of RECO and they generally show similar dynamics (Bond-Lamberty et al., 2018; Barba et al., 2018). Using the Soil Respiration Database (SRDB) version 5 (Jian et al., 2021), we extracted R_H:R_S ratios averaged by PFT and used these to calculate the R_H fraction of COSORE-reported R_S, based on matching PFT classes. Those ratios are consistent with the analysis of Bond-Lamberty et al. (Table S6). COSORE datasets that reported negative SM or SM $< 0.02\, m^3\, m^{-3}$ were excluded from the analysis. Few COSORE sites report the depth of collar insertion; all have recorded depths $\leq$ 10 cm. We computed the median R_S flux, converted from $\mu mol\ CO_2\, m^{-2}\, s^{-1}$ to $g\, C\, m^{-2}\, s^{-1}$ using the molar mass of carbon, across ports.

After filtering COSORE datasets on these criteria, we split them into two groups. In the first group, 13 COSORE datasets (Chang et al., 2008; Carbone et al., 2011, 2013; Ataka et al., 2014; Sánchez-Cañete et al., 2016; Vargas et al., 2018) reported concurrent,

daily SM, temperature, and R_S flux values (Table S1). These *in situ* SM and temperature data are most appropriate for modeling at COSORE sites given the relatively coarse scale of TCF input datasets. Soil texture and porosity data were obtained for these sites from the Catchment model. We computed a 365-day GPP climatology from SMAP L4C Version 5 dataset (2015-2019) at each COSORE location. Use of a GPP climatology eliminates canopy changes, real or spurious, that may not be reflected in the respiration measurements from COSORE chamber studies due to the scale mismatch. For experiments that included a CASA litterfall phenology, the daily litterfall fraction was computed as the average across EC tower sites for each PFT class.

A key issue arises with using COSORE-reported driver data in TCF models calibrated on L4SM, as SM values generated by one model (or measured in the field) are generally not comparable with those derived from another (Koster et al., 2009). The small number of relevant COSORE datasets precludes re-calibration of TCF using COSORE observations. Instead, we applied a bias correction, using an affine statistical transformation to re-scale COSORE moisture and temperature values to match the L4SM data based on within-PFT means. The coefficients from a linear regression of rank-ordered L4SM values on rank-ordered COSORE values were applied to transform the COSORE values of sites based on their PFT (i.e., slope parameter varying with PFT). We mapped the COSORE-reported biome to MOD12Q1 PFTs, which were often identical. To obtain a continuous record of soil moisture and temperature (required for TCF model operation), a daily COSORE climatology, by PFT, was used to fill-in missing values.

The second group of COSORE datasets consists of 12 other sites (Curtis et al., 2005; Baldocchi et al., 2006; Jassal et al., 2008; Noormets et al., 2010; Detto et al., 2013; Gaumont-Guay et al., 2014; Zhang et al., 2018; Ueyama et al., 2018) located within 9 km of a FLUXNET tower. Although these 12 datasets did not include driver data, we compared the modeled R_H flux (based on L4SM and MERRA-2 driver data) from those nearby FLUXNET sites, for each experiment, to the (partitioned) R_H flux from COSORE.

3 Results

Each modification to the R_H and/or SOC sub-models produced a meaningful improvement in the estimated RECO and NEE seasonal cycles relative to the TCF NRv8.3 model baseline with no modifications (Figure 2). The modification to the R_A model, via the Kok effect, produced no discernible improvement in the seasonal cycles (Tables 1, 2). The mean day-of-year (DOY) of the NEE minimum (RECO maximum) for the high northern latitudes ($\geq$ 40 degrees N latitude), based on filtering of tower data (Table S2), is estimated to be 181 (197). Depending on the method used to quantify the phase difference (Tables S2, S3), in NRv8.3 the NEE minimum (RECO maximum) is delayed (advanced) by 15-26 days (12-14 days). This aggregate seasonal cycle obscures underlying heterogeneity but is useful as a high-level diagnostic. Some PFTs show a stronger phase correction than others (Figure 3). Spatial variation in the timing of the NEE minimum due to PFT and climate can be observed if we apply the TCF model at global extent (Figure 4).

The Fourier regression (Table S3) and low-pass filter results (Table S2) agree broadly as to the effect of each modification on the overall fit to the seasonal cycle of the EC flux towers; i.e., each intervention, other than the Kok effect, produces a meaningful model improvement. However, they disagree substantially as to the length of the time lag for all PFTs except ENF (Tables 2 and S3). Some of this difference can be attributed to the lack of strong periodicity in NEE for some PFTs (e.g., SHB, GRS) which can confound the Fourier regression results; conversely, PFTs with broad seasonal peaks/ troughs (e.g., CCR, BCR) may confound the low-pass filter. Differences in the TCF model fit parameters (if re-calibrated) and other observations unique to each experiment are reported below.

Table 1: Difference (experiment minus Tower observations) in day-of-year (DOY) of NEE minimum (maximum net ecosystem carbon uptake), in days, for each experiment, based on the mean NEE seasonal cycle, smoothed with a low-pass filter using a 7-day moving window, for all sites above 40 degrees N latitude.

Product	ENF	DNF	DBF	SHB	GRS	CCR	BCR
NRv8.3	+26	+19	+16	+5	+4	+12	+15
NRv8.3 + Kok Effect	+26	+19	+16	+4	+4	+12	+15
NRv8.3 + O2 Limit	+14	+18	+3	-5	+4	+11	+1
NRv8.3 + Litterfall Phenology	+13	+18	+1	+3	+3	+10	-1
NRv8.3 + Soil Profile	+26	+17	+4	+3	+4	+10	+1
NRv8.3 + O2 Limit + Litterfall	+12	+18	+1	-6	-5	+10	+0
NRv8.3 + Soil Profile + O2 Limit	+28	+17	+4	+4	+6	+10	-1
NRv8.3 + Soil Profile + Litterfall	+13	+17	+2	+3	+4	+10	+0
NRv8.3 + Soil Profile + O2 Limit + Litterfall	+26	+17	+2	+4	+6	+10	-2

Table 2: Difference (experiment minus Tower observations) in day-of-year (DOY) of RECO maximum, in days, for each experiment, based on the mean RECO seasonal cycle, smoothed with a low-pass filter using a 7-day moving window, for all sites above 40 degrees N latitude.

Product	ENF	DNF	DBF	SHB	GRS	CCR	BCR
NRv8.3	-13	-34	-17	-2	-10	-13	-36
NRv8.3 + Kok Effect	-12	-34	-17	-2	-10	-13	-18
NRv8.3 + O2 Limit	-6	-34	-13	+0	+1	-9	-17
NRv8.3 + Litterfall Phenology	-5	-34	+3	+0	+19	+3	+32
NRv8.3 + Soil Profile	-12	-9	-17	+0	-9	-9	-17
NRv8.3 + O2 Limit + Litterfall	-4	-10	+0	+1	+4	-4	+9
NRv8.3 + Soil Profile + O2 Limit	-13	-9	-14	-2	+0	-8	-2
NRv8.3 + Soil Profile + Litterfall	-5	-9	-13	+0	+6	+3	+2
NRv8.3 + Soil Profile + O2 Limit + Litterfall	-12	-9	-13	-1	+0	+3	-1

3.1 Single-Factor Experiments

3.1.1 NRv8.3 + Litterfall Phenology

A seasonally varying litterfall scheme produced the best joint improvement in the NEE and RECO seasonal cycles (Table S2), relative to NRv8.3, particularly for DBF (Tables 1, 2). The NEE seasonal cycle of DBF, with the new litterfall scheme, is almost a perfect match to the tower record (despite a bias difference), including the autumn increase in CO_2 flux to the atmosphere. This autumnal increase is also shown in the modeled NEE results for the BCR PFT, but it is not apparent in the corresponding tower data. Conversely, NRv8.3 shows a spurious high NEE anomaly for BCR in spring that is eliminated by this experiment's considerable shift in the BCR RECO seasonal cycle (Figure S3).

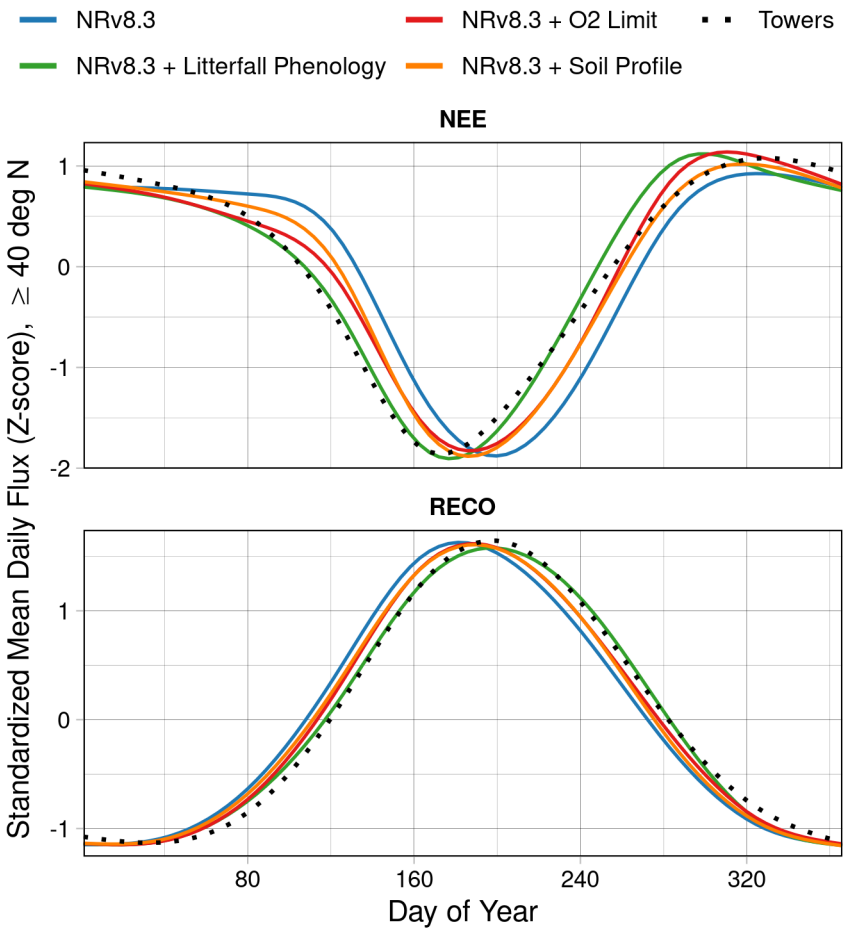

Figure 2. Mean seasonal RECO and NEE cycles for each experiment and for the EC flux towers ("Towers"), shown with smoothing b-splines, for all sites north of 40 degrees N latitude. The NRv8.3 + Kok Effect experiment is not shown because it overplots the NRv8.3 baseline almost exactly.

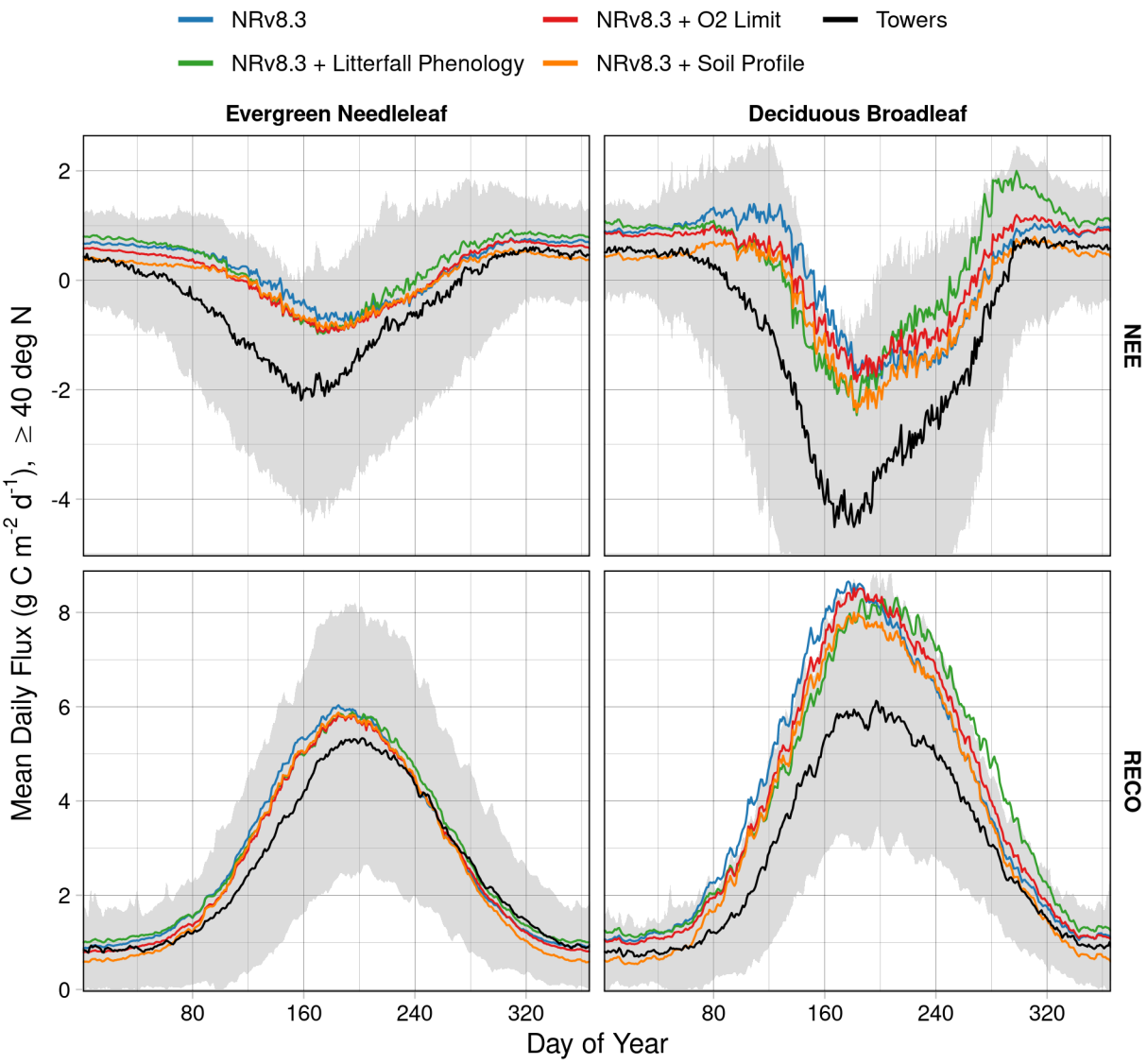

Figure 3. Mean seasonal RECO and NEE cycles for each experiment and for the EC flux towers ("Towers") at tower sites north of 40 degrees N latitude for the ENF and DBF PFTs. The shaded area shows one spatial standard deviation for the Towers and is clipped for DBF NEE. Plots of the mean seasonal cycles for each PFT, separately, are available in the Supplement.

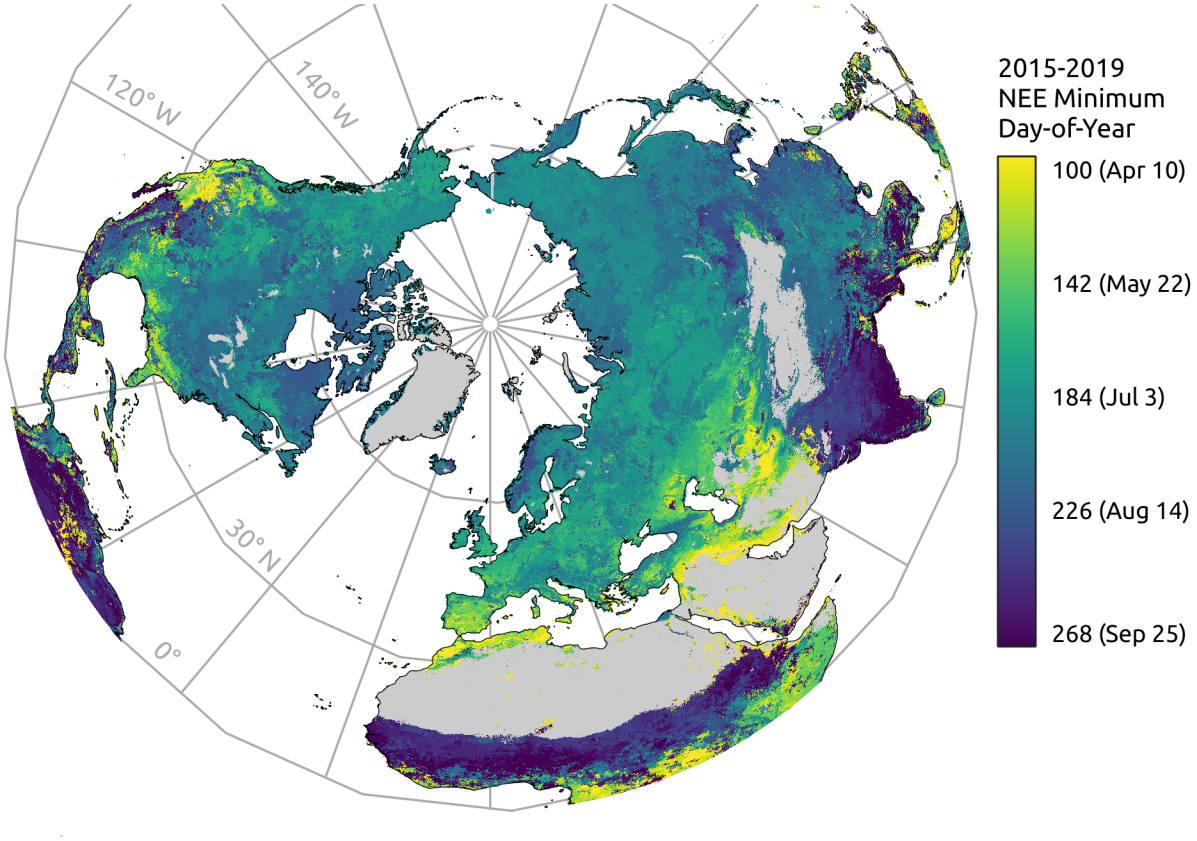

Figure 4. Map of the day-of-year on which the minimum net ecosystem exchange (NEE) occurs, based on the average 2015-2019 seasonal cycle of NEE from SMAP L4C Version 5 product, which incorporates the TCF model. Areas outside the model domain are shown in gray and white.

3.1.2 NRv8.3 + O2 Limit

With the O_2 diffusion limit, all PFTs show reduced NEE magnitude and most show less RECO throughout most of the year, though increased RECO is observed in the fall for some PFTs, particularly DBF (Figure 3). The RECO seasonal cycle is improved for ENF, DBF, SHB, and cropland PFTs. As with the new litterfall scheme, the addition of an O_2 diffusion limit eliminated a spurious spring NEE anomaly for BCR in NRv8.3 (Figure S4). But unlike the new litterfall scheme, the O_2 diffusion limit did *not* introduce a spurious autumnal NEE anomaly for BCR (Figures S3 and S4). In general, the resulting phase correction in RECO is not as strong as in the NRv8.3 + Litterfall Phenology experiment (Figure S3). Looking at the residuals (compared to tower observations), NRv8.3 over-estimates RECO at high SM in ENF, GRS, and croplands. Adding an O_2 diffusion limit reduces that high bias; however, in the NRv8.3 + O2 Limit experiment, GRS and DBF show a slight under-estimation of RECO at high SM.

3.1.3 NRv8.3 + Soil Profile

The NRv8.3 + Soil Profile experiment produced only a moderate correction to the NEE and RECO seasonal cycles. We experimented with different functional forms for the litterfall input distribution and R_H extinction function, $h(z)$ (Equation 7). For the litterfall inputs, as Koven et al. also suggested, we evaluated profiles based on the root profiles of Jackson et al., a root density profile based on the Community Land Model (Lawrence et al., 2019), and the normalized, median SOC profile from SoilGrids 250m (Hengl et al., 2017) (Figure S16). The negative exponential $h(z)$ better matched the shape of the median SoilGrids 250m profile and, in anticipation of a high RECO bias due to high SOC storage, we reduced the SOC storage magnitude by using a 9-cm e-folding depth (Figure S18), instead of 10-cm as suggested by Koven et al.. As expected, SOC storage increases with a multi-layer soil model (Figure S19).

3.1.4 NRv8.3 + Kok Effect

Plant CUE was much lower in the re-calibrated BPLUT when the Kok effect was applied, with values in the range [0.38, 0.70] across PFTs compared to [0.53, 0.78] in NRv8.3. Accordingly, RECO in the Kok effect experiment is partitioned very differently from NRv8.3, with a general decline in R_H but an increase in R_A. Despite this change, the overall RECO level is very similar to that of NRv8.3 and the seasonal cycles of NEE and RECO are unchanged. The apparent improvement for the BCR PFT (Table 2) is likely spurious due to a broad, flat minimum NEE for that PFT's seasonal cycle.

3.2 Factorial Combinations

In addition to single-factor experiments, we ran experiments in which multiple factors were combined, with the exception of the Kok effect implementation, as that experiment did not show improvement in the timing of the mean seasonal cycles. For the NRv8.3 + O2 Limit + Litterfall multi-factor experiment, no re-calibration was necessary, as the NRv8.3 + O2 Limit parameters were re-used. The NRv8.3 + Soil Profile + O2 Limit experiment did require re-calibration. The experiment combining both an O_2 limit and litterfall phenology generally resembles an average of those single-factor experiments (Figure S8). Interestingly, the NRv8.3 + O2 Limit + Litterfall experiment yields the most substantial correction of all multi-factor experiments and a substantial improvement in the RECO and NEE seasonal cycles for ENF compared to the single-factor experiments.

Where an O_2 limit and vertical soil profile were combined, the steady-state SOC storage was unreasonably high, with total-column SOC content exceeding 870 kg m^-2 and surface-layer (0-5 cm) SOC density of around 120 kg m^{-3}. Non-exponential litterfall input functions combined with the power-law R_H extinction function yielded smaller,

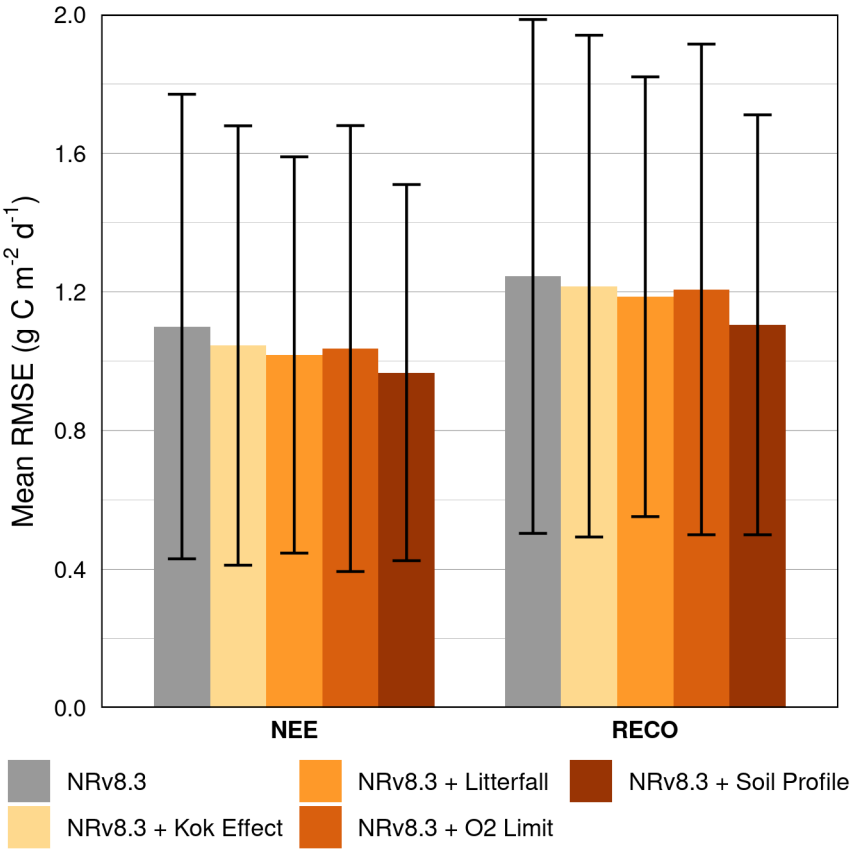

Figure 5. Root mean-squared error (RMSE) of modeled NEE, RECO fluxes versus observed fluxes at the 26 L4C Core Validation EC tower Sites (CVS) for the single-factor experiments. Error bars show one standard deviation across EC tower sites.

more realistic steady-state SOC pools, but failed to improve the RECO and NEE skill. The NRv8.3 + Soil Profile + Litterfall experiment, however, improved upon the baseline and the respective single-factor experiments; notably, an autumn high bias in the NEE cycles of DBF and BCR in the NRv8.3 + Litterfall experiment was much reduced (Figures S3, S7).

3.3 Validation against Tower and Chamber Datasets

Modeled fluxes from each single-factor experiment compared well to the observed NEE, RECO fluxes at the L4C CVS (Figure 5). Some of these sites are located below 40 degrees N latitude, including the southern hemisphere, and therefore indicate that none of the new respiration mechanisms, as single factors, results in degraded NEE or RECO skill relative to the baseline NRv8.3. Conversely, in the combined experiments, the combination of an O_2 diffusion limit with other changes to the R_H model led to degraded NEE and RECO skill (Figure 6).

Compared to FLUXCOM, the NRv8.3 + O2 Limit showed the best agreement in the RECO and NEE seasonal cycles, though the NRv8.3 + Soil Profile and NRv8.3 + Soil Profile + Litterfall experiments also compare well (Tables 3, S5). Both phase estimation approaches agree that the single-factor experiments (other than NRv8.3 + Kok Effect) match the FLUXCOM seasonal cycles of RECO and NEE better than the base-

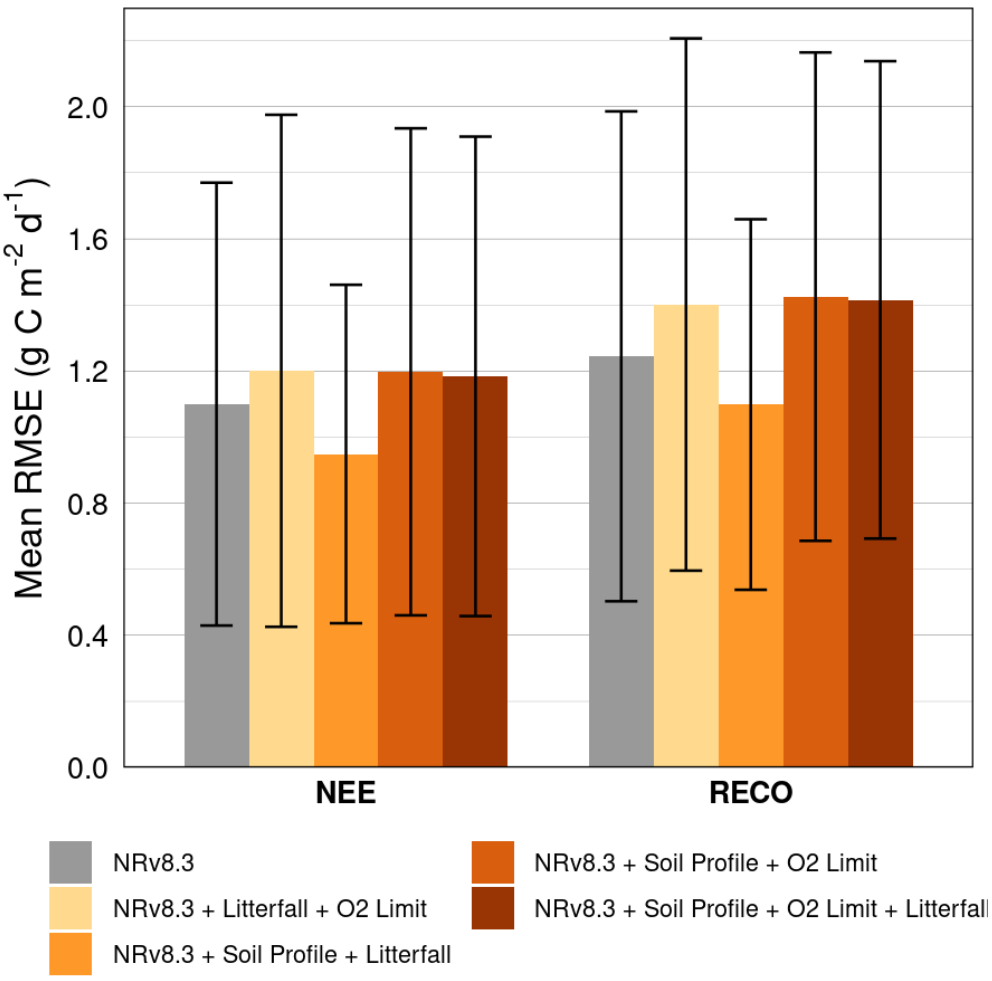

Figure 6. Root mean-squared error (RMSE) of modeled NEE, RECO fluxes versus observed fluxes at the 26 L4C Core Validation EC tower Sites (CVS) for the experiments with combinations of factors. Error bars show one standard deviation across EC tower sites.

line NRv8.3 product; however, they disagree considerably about the multi-factor experiments and the apparent residual lead in the RECO seasonal cycle (Table 3).

The modeled results at COSORE sites, combining those with independent driver data and those that are within an EC tower footprint, indicate that every experiment, other than NRv8.3 + Kok Effect, improved upon the NRv8.3 baseline in terms of R_H modeling skill (Table 4). The experiment with a vertical soil profile, with or without a litterfall phenology, produced an improvement in the R_H anomaly correlation and the greatest improvement in all skill metrics. The O_2 diffusion limitation, in particular, produced a substantial improvement in R_H RMSE and biased-adjusted RMSE (ubRMSE) that can be attributed primarily to the substantial reduction in high-R_H residuals at high SM (Figure S10). The improvement in the NRv8.3 + O2 Limit experiment is notable at one moist, high-elevation ENF site (Chang et al., 2008); NRv8.3 and all other experiments fail to accurately simulate R_H dynamics at this site (median $r = 0.15$; median anomaly $r = 0.50$) but, with the O_2 limit, TCF simulates R_H with very high accuracy, including spikes in R_H during dry-downs ($r = 0.88$; anomaly $r = 0.85$; Figures S20 and S21).

4 Discussion

Three different modifications to the TCF soil decomposition model resulted in substantial corrections to the modeled seasonal carbon cycles in the NH and improved overall RECO and NEE modeling skill. Of the singular modifications tested, a seasonally varying litterfall scheme resulted in the greatest, consistent improvement in the RECO and NEE phase across PFTs. As that experiment involved no model re-calibration or new parameterization, we can attribute that improvement to the relative change in SOC substrate availability for R_H. In contrast, the moderate improvements in RECO and associated NEE phase under the O_2 diffusion limitation and vertical soil profile experiments seem to have resulted from an overall reduction in RECO, particularly during the NH spring (Figure 3). Seasonally varying litterfall was most effective at reducing the phase bias in DBF, while an O_2 limit was most effective in GRS; both were effective in ENF. The vertical soil profile was much less effective at reducing either RECO or NEE phase bias in most PFTs, though it did mitigate bias in croplands and improved overall modeling skill (Table 4).

It should be noted that the high NH RECO bias of TCF is a major contributing factor to the NEE phase bias; as the modeled GPP cycle is tied to satellite observations and fixed in each experiment, merely reducing the RECO magnitude would result in a phase shift of the NEE cycle. In the NH, the NEE cycle would be advanced (i.e., shifted earlier in time). We verified the role of RECO magnitude in the TCF simulations, by inflating tower RECO 25%, and then re-calculating NEE using NRv8.3 GPP. Consequently, while an NEE phase correction may result from the reduction of a bias in RECO magnitude, we can interpret a RECO phase correction as an improvement in the timing of respiration phenology. To verify the mechanisms tested here, we examined the change in the RECO residual (difference in residual between modeled and observed RECO) for each experiment compared to the baseline NRv8.3 (Figures S11-S14). The experiments that were successful at correcting the RECO seasonal cycle all showed substantially reduced RECO during the NH spring months (April, May, June), particularly for the DBF and cropland PFTs. With the exception of the NRv8.3 + Kok Effect experiment, which failed to mitigate RECO bias, each experiment reduced the spring RECO bias in a different way.

The O_2 diffusion limitation produced the greatest reduction in residual RECO at both low and high values of soil moisture (SM), particularly in spring (Figure S13), suggesting that an optimum SM exists for soil heterotrophs, at least when antecedent SM conditions are not taken into account (Ryan et al., 2015; Sihi et al., 2018). An upper limit

Table 3: Day-of-year (DOY) of NEE minimum, RECO maximum for FLUXCOM, EC flux towers ("Towers"), and experiments along with the difference in DOY (experiment/ Towers minus FLUXCOM), in days, for Towers, NRv8.3, and each experiment, identified using a low-pass filter, for the land domain above 40 degrees N latitude (FLUXCOM) or EC flux tower sites above 40 degrees N latitude.

Product	Peak RECO DOY	Peak NEE DOY	RECO Phase (days)	NEE Phase (days)
FLUXCOM	195	183	n.a.	n.a.
Towers	197	181	+2	-2
NRv8.3	183	196	-12	+13
NRv8.3 + Kok Effect	184	196	-11	+13
NRv8.3 + Litterfall Phenology	187	182	-8	-1
NRv8.3 + O2 Limit	186	186	-9	+3
NRv8.3 + Soil Profile	185	186	-10	+3
NRv8.3 + O2 Limit + Litterfall	187	182	-8	-1
NRv8.3 + Soil Profile + Litterfall	186	183	-9	+0
NRv8.3 + Soil Profile + O2 Limit	186	186	-9	+3
NRv8.3 + Soil Profile + O2 Limit + Litterfall	186	183	-9	+0

Table 4: For each experiment, the average root mean-squared error (RMSE), average unbiased RMSE (ubRMSE), median Pearson's correlation (r), and median r for demeaned anomalies, across sites, against the observed COSORE R_H flux. Standard deviation across sites is noted for RMSE, ubRMSE in parentheses. Significant improvements in correlation, relative to NRv8.3, are denoted: *** (p-value < 0.01), ** (p-value < 0.05), * (p-value < 0.1).

Product	Num. Sites	RMSE	ubRMSE	Correlation (r)	Anomaly r
NRv8.3	25	2.04 (±0.99)	0.68 (±0.42)	0.630	0.390
NRv8.3 + Kok Effect	25	1.77 (±0.83)	0.65 (±0.41)	0.631	0.389
NRv8.3 + Litterfall Phenology	25	1.99 (±0.94)	0.69 (±0.43)	***0.687	0.369
NRv8.3 + O2 Limit	25	1.58 (±0.65)	0.65 (±0.41)	***0.687	0.383
NRv8.3 + O2 Limit + Litterfall	25	1.87 (±0.88)	0.66 (±0.43)	***0.659	0.377
NRv8.3 + Soil Profile	25	1.31 (±0.67)	0.62 (±0.40)	***0.746	***0.438
NRv8.3 + Soil Profile + Litterfall	25	1.28 (±0.67)	0.62 (±0.40)	***0.750	***0.441
NRv8.3 + Soil Profile + O2 Limit	25	1.55 (±0.93)	0.80 (±0.49)	***0.655	0.369
NRv8.3 + Soil Profile + O2 Limit + Litterfall	25	1.55 (±0.93)	0.80 (±0.49)	***0.657	0.361

on the response of R_H to soil moisture has been shown to improve modeled RH estimates (Ťupek et al., 2019) and, as our results at COSORE sites indicate, specifically improves estimates at sites that experience high soil moisture conditions and at one alpine ENF site (Table 4 and Figure S10). When the O_2 diffusion limit is combined with a linear or sub-linear function that increases with soil moisture (i.e., representing greater substrate availability), the result is a triangular function with a fairly narrow range of optimum soil moisture, which agrees with the observation that SM is most limiting on R_H when soils are relatively dry or approaching saturation (Reichstein et al., 2003). At high northern latitudes, these conditions may predominate during spring thaw (Oikawa et al., 2014; Winnick et al., 2020), which underscores the key role of SM in accurately modeling the corresponding carbon cycle transitions.

The new litterfall allocation scheme shows a similar spring reduction in the RECO residual but it is not patterned by soil moisture or temperature (Figure S12). Instead, there is a temporal pattern: residual RECO is reduced in the first half of the year but is elevated during the second half, effectively reducing R_H and RECO in spring just as an O_2 diffusion limitation does when SM is high. The fall RECO increase then results from a release from substrate limitation (Leitner et al., 2016; Nielsen et al., 2019). The CASA model (Randerson et al., 1996), from which our litterfall scheme is derived, displays RECO and NEE phase biases similar to TCF (Byrne et al., 2018, Figure 2). This is particularly interesting as the NRv8.3 + Litterfall Phenology experiment considerably improved the phase offset between TCF and the tower observations (Tables 1, 2) and perhaps over-corrected when compared to FLUXCOM (Table S4). Randerson et al. noted the CASA litterfall scheme led to an advanced R_H seasonal cycle (earlier peak), which was expected due to a build-up of fall substrate inputs and, in turn, a high substrate availability in spring (Byrne et al., 2018). However, in our experiment, the same litterfall scheme only delayed the R_H cycle. This discrepancy depends on whether or not winter-time R_H is sufficiently reduced, relative to litterfall inputs, so as to allow substrate pools to increase before spring. Another key difference between CASA and TCF is the much coarser spatial resolution of CASA (and coarser temporal resolution in Randerson et al., 1996).

When we look at the difference in RECO residuals from the NRv8.3 + Kok Effect experiment, stratified by PAR, the RECO residual is still high at almost all levels of PAR but especially when PAR is high, indicating that a CUE response to PAR is not having the intended effect on the seasonal cycle (Figure S11). This may be due to TCF's high RECO bias in the NH (Figure 3), i.e., the R_A fraction increases to the extent that R_H is reduced, resulting in a similar level of RECO to NRv8.3. This intrinsic high bias in RECO may be due to the night-time partitioning of EC tower fluxes (Keenan et al., 2019). Alternatively, or in addition to this problem, there may be a problem with our implementation of a PAR scalar modulating CUE at daily time scale, as R_A is known to continue throughout the day and sub-daily co-variation of PAR and temperature is considerable (Heskel et al., 2013; Peng et al., 2013); TCF's use of daily average meteorology that is more representative of daytime conditions may contribute to the high RECO bias (Wehr et al., 2016).

Despite its small effect on the mean seasonal cycles, the greatest improvement in both NEE and RECO modeling skill (Figure 5) came from the incorporation of a vertical soil profile into the TCF soil decomposition model. The small correction in phase bias seems to be due to the lagged R_H flux that arises from the slow diffusion of heat and, to a lesser extent, of moisture through the soil column. We verified this mechanism by plotting the standardized, modeled R_H flux in each soil layer from the NRv8.3 + Soil Profile experiment, along with the (single-layer) flux from NRv8.3 (Figure S15). The results indicate that, with a vertically stratified soil decomposition model, the individual-layer R_H fluxes are lagged and decline in magnitude with increasing soil depth. Consequently, the whole-column, total R_H flux in the vertically resolved model approaches the magnitude of the single-layer model, though the multi-layer total is slightly smaller. The

result is that the NEE and RECO cycles both peak in early July (Table S2) but the RECO peak is broader, consistent with Yi et al.. In mid-to-late summer, the RECO flux at the NH sites is substantially reduced due to SM (i.e., substrate diffusion) limits (not shown).

This lag effect and corresponding improvement in the RECO seasonal cycle could be enhanced if deeper soil layers were modeled with higher SOC storage. In the NRv8.3 + Soil Profile experiment, SOC storage diminishes to almost zero at 1.5 and 3-m depth. The exponentially declining input distribution of Koven et al. is a good match for the median, global SOC profile from SoilGrids 250m (Figure S16) as well as the distribution of carbon by age (Balesdent et al., 2018); however, TCF depletes deep SOC storage during model spin-up (Figure S18). This underscores that further improvements to effectively model SOC protection mechanisms are needed in order to accurately simulate R_H fluxes from a multi-layer soil decomposition model. The exponential litterfall distributions that allocate very little SOC to deeper layers (Figure S16) are probably more realistic than distributions based on root fractions (Shi et al., 2020). However, an exponential extinction of R_H with depth may not be reasonable, as there is recent evidence that between 30-60% of CO_2 efflux originates below 1 m depth (Wan et al., 2018). For simplicity, our model varies neither the turnover times nor the environmental response functions with depth. Addressing these limitations will require improved data on the vertical distribution of R_H flux.

In TCF, calibrating SOC turnover is somewhat subjective, as the base decay rates are determined by comparing the inferred SOC storage from inverting the R_H flux with that indicated by the International Geosphere-Biosphere Data and Information System (IGBP-DIS) soil inventory record (Global Soil Data Task Group, 2000). However, the base rates likely should be modified when soil decomposition mechanisms are changed and should probably vary with soil layer depth; doing so might result in more favorable RECO, NEE skill metrics for the multi-factor experiments (Figure 6). Another limitation in this study is the neglect of GPP magnitude bias. Although the phase of GPP is expected to be constrained by the satellite-observed fPAR (Messerschmidt et al., 2013), a GPP magnitude bias also has the potential to introduce an NEE phase bias and requires further research along the same lines of this study.

The model enhancements produce similar phase corrections when results from different PFTs are pooled. This equifinality suggests that the modifications to TCF assessed here may not be equally relevant to all PFTs. For instance, the new litterfall scheme resulted in a better match to autumnal NEE for DBF but also created a spurious high NEE anomaly in autumn for BCR. The combination of O_2 limit and vertical soil profile also further delayed (advanced) the mean NEE (RECO) seasonal cycle for ENF. The equifinality among experiments also indicates that the NH seasonal cycle of NEE is an emergent property of terrestrial ecosystems (Birch et al., 2021) and that we are likely missing some interactions between limiting factors and driving relationships of soil decomposition, e.g., microbial biomass and stabilization of SOC (Johnston & Sibly, 2018) or litter input traits (Hu et al., 2018). After all, there is some residual misfit in the modeled seasonal cycles (Tables 1, 2) and TCF still retains a high RECO bias. In addition to the high residual RECO bias, which may be due to the partitioning of EC tower fluxes, TCF also has a relatively large NEE magnitude bias, as its summer-time GPP and NEE amplitudes are smaller than tower observations (Figure 3). Future development of TCF and similar models—given their promise for global, operational terrestrial carbon budgeting (e.g., SMAP L4C)—should focus on reducing RECO bias, starting with an assessment of different EC flux partitioning methods (Keenan et al., 2019) and SOC protection mechanisms.

5 Conclusions

A seasonally varying adjustment of R_H model processes, including the litterfall allocation to SOC available for decomposition, resulted in major corrections to the modeled RECO and NEE seasonal cycles, as compared to EC flux tower observations, in a first-order soil decomposition model. An explicit litterfall phenology, with or without a vertically resolved SOC decomposition model, yields the best improvement in phase. The NEE phase bias in TCF for high northern latitude sites ($\geq$ 40 N), was reduced from a lag of 15-26 days to between a 5-day lead or 15-day lag, depending on the experiment. Based on a comparison to the FLUXCOM seasonal cycle above 40 degrees N latitude, the model enhancements generally eliminated the NEE phase bias, though a smaller RECO phase bias remains. Comparison to independent, *in situ* chamber measurements indicates the proposed mechanisms can improve RECO and NEE modeling skill.

The RECO phase bias can result from a bias in RECO magnitude, i.e., from excess modeled autotrophic (R_A) or heterotrophic respiration (R_H) at key seasonal intervals. Two model enhancements, adding a limit on O_2 diffusion for soil heterotrophs or a seasonally varying litterfall inputs scheme, reduced the phase biases in RECO and NEE by reducing R_H during the NH spring season. The O_2 limit restricts R_H as soil moisture increases, which is common in the NH spring in many regions due to snowmelt and increased rainfall. The new litterfall scheme directly shifts the R_H seasonal cycle later in time by enhancing substrate limitation in the spring. Although less effective at correcting RECO or NEE phase bias, a multi-layer soil decomposition model also reduced spring NH RECO. This is due to lagged R_H flux from deeper soil layers, effectively amortizing the whole-column R_H flux over a longer period.

Accurate timing of the terrestrial NEE cycle is key if such modeled estimates are to be used as priors in atmospheric inversion studies. Moreover, the NEE seasonal cycle, observed by EC flux towers or estimated in data-driven syntheses, can be used to diagnose missing or poorly represented model processes. Going forward, increased *in situ* monitoring of soil respiration fluxes—particularly vertically resolved fluxes—of soil organic carbon, and of below-ground R_A will be essential for constraining modeled soil respiration in terrestrial carbon flux models.

Acknowledgments

The authors would like to thank Randal D. Koster (Global Modeling and Assimilation Office, NASA Goddard Space Flight Center) for his feedback on the soil hydrology model and the paper. This study was supported with funding from NASA (NX14AI50G, 80NSSC19M0114). The SMAP L4C operational product (Version 5) is publicly accessible through the National Snow and Ice Data Center (NSIDC) at `https://nsidc.org/data/SPL4CMDL/versions/5`. The TCF model code is available online at `https://github.com/arthur-e/pyl4c`. The soil hydrology model code is available at `https://github.com/arthur-e/simsoil`.

References

Alexandrov, G. A. (2014). Explaining the seasonal cycle of the globally averaged CO2 with a carbon-cycle model. *Earth System Dynamics*, *5*(2), 345–354. doi: 10.5194/esd-5-345-2014

Ataka, M., Kominami, Y., Yoshimura, K., Miyama, T., Jomura, M., & Tani, M. (2014, oct). In Situ CO2 Efflux from Leaf Litter Layer Showed Large Temporal Variation Induced by Rapid Wetting and Drying Cycle. *PLoS ONE*, *9*(10), e108404. Retrieved from `https://dx.plos.org/10.1371/journal.pone.0108404` doi: 10.1371/journal.pone.0108404

Baldocchi, D. (2008). 'Breathing' of the terrestrial biosphere: lessons learned from a global network of carbon dioxide flux measurement systems. *Australian Journal of Botany*, *56*(1), 1. Retrieved from http://www.publish.csiro.au/?paper=BT07151 doi: 10.1071/BT07151

Baldocchi, D., Tang, J., & Xu, L. (2006, jun). How switches and lags in biophysical regulators affect spatial-temporal variation of soil respiration in an oak-grass savanna. *Journal of Geophysical Research: Biogeosciences*, *111*(G2), n/a–n/a. Retrieved from http://doi.wiley.com/10.1029/2005JG000063 doi: 10.1029/2005JG000063

Balesdent, J., Basile-Doelsch, I., Chadoeuf, J., Cornu, S., Derrien, D., Fekiacova, Z., & Hatté, C. (2018, jul). Atmosphere–soil carbon transfer as a function of soil depth. *Nature*, *559*(7715), 599–602. Retrieved from https://www.cambridge.org/core/product/identifier/9781139029339{\%}23CN-bp-6/type/book{_}parthttp://www.nature.com/articles/s41586-018-0328-3 doi: 10.1038/s41586-018-0328-3

Barba, J., Cueva, A., Bahn, M., Barron-Gafford, G. A., Bond-Lamberty, B., Hanson, P. J., ... Vargas, R. (2018). Comparing ecosystem and soil respiration: Review and key challenges of tower-based and soil measurements. *Agricultural and Forest Meteorology*, *249*(March 2017), 434–443. doi: 10.1016/j.agrformet.2017.10.028

Birch, L., Schwalm, C. R., Natali, S., Lombardozzi, D., Keppel-Aleks, G., Watts, J., ... Rogers, B. M. (2021, jun). Addressing biases in Arctic–boreal carbon cycling in the Community Land Model Version 5. *Geoscientific Model Development*, *14*(6), 3361–3382. Retrieved from https://gmd.copernicus.org/articles/14/3361/2021/ doi: 10.5194/gmd-14-3361-2021

Bond-Lamberty, B., Bailey, V. L., Chen, M., Gough, C. M., & Vargas, R. (2018). Globally rising soil heterotrophic respiration over recent decades. *Nature*, *560*(7716), 80–83. Retrieved from http://dx.doi.org/10.1038/s41586-018-0358-x doi: 10.1038/s41586-018-0358-x

Bond-Lamberty, B., Epron, D., Harden, J., Harmon, M. E., Hoffman, F., Kumar, J., ... Vargas, R. (2016). Estimating heterotrophic respiration at large scales: Challenges, approaches, and next steps. *Ecosphere*, *7*(6), 1–13. doi: 10.1002/ecs2.1380

Bond-Lamberty, B., Christianson, D. S., Malhotra, A., Pennington, S. C., Sihi, D., AghaKouchak, A., ... Zou, J. (2020, dec). COSORE: A community database for continuous soil respiration and other soil-atmosphere greenhouse gas flux data. *Global Change Biology*, *26*(12), 7268–7283. Retrieved from https://onlinelibrary.wiley.com/doi/10.1111/gcb.15353 doi: 10.1111/gcb.15353

Byrne, B., Wunch, D., Jones, D. B., Strong, K., Deng, F., Baker, I., ... Roehl, C. M. (2018). Evaluating GPP and respiration estimates over northern midlatitude ecosystems using solar-induced fluorescence and atmospheric CO2 measurements. *Journal of Geophysical Research: Biogeosciences*, *123*(9), 2976–2997. doi: 10.1029/2018JG004472

Carbone, M. S., Park Williams, A., Ambrose, A. R., Boot, C. M., Bradley, E. S., Dawson, T. E., ... Still, C. J. (2013, feb). Cloud shading and fog drip influence the metabolism of a coastal pine ecosystem. *Global Change Biology*, *19*(2), 484–497. Retrieved from https://onlinelibrary.wiley.com/doi/10.1111/gcb.12054 doi: 10.1111/gcb.12054

Carbone, M. S., Still, C. J., Ambrose, A. R., Dawson, T. E., Williams, A. P., Boot, C. M., ... Schimel, J. P. (2011, sep). Seasonal and episodic moisture controls on plant and microbial contributions to soil respiration. *Oecologia*, *167*(1), 265–278. Retrieved from http://link.springer.com/10.1007/s00442-011-1975-3 doi: 10.1007/s00442-011-1975-3

Chang, S.-C., Tseng, K.-H., Hsia, Y.-J., Wang, C.-P., & Wu, J.-T. (2008, may). Soil

respiration in a subtropical montane cloud forest in Taiwan. *Agricultural and Forest Meteorology*, *148*(5), 788–798. Retrieved from https://linkinghub.elsevier.com/retrieve/pii/S0168192308000026 doi: 10.1016/j.agrformet.2008.01.003

Chapin, F. S., Woodwell, G. M., Randerson, J. T., Rastetter, E. B., Lovett, G. M., Baldocchi, D. D., ... Schulze, E. D. (2006, nov). Reconciling carbon-cycle concepts, terminology, and methods. *Ecosystems*, *9*(7), 1041–1050. Retrieved from http://link.springer.com/10.1007/s10021-005-0105-7 doi: 10.1007/s10021-005-0105-7

Ciais, P., Tan, J., Wang, X., Roedenbeck, C., Chevallier, F., Piao, S. L., ... Tans, P. (2019). Five decades of northern land carbon uptake revealed by the interhemispheric CO2 gradient. *Nature*, *568*(7751), 221–225. Retrieved from http://dx.doi.org/10.1038/s41586-019-1078-6 doi: 10.1038/s41586-019-1078-6

Curtis, P. S., Vogel, C. S., Gough, C. M., Schmid, H. P., Su, H.-B., & Bovard, B. D. (2005, aug). Respiratory carbon losses and the carbon-use efficiency of a northern hardwood forest, 1999–2003. *New Phytologist*, *167*(2), 437–456. Retrieved from https://onlinelibrary.wiley.com/doi/10.1111/j.1469-8137.2005.01438.x doi: 10.1111/j.1469-8137.2005.01438.x

Davidson, E. A., Richardson, A. D., Savage, K. E., & Hollinger, D. Y. (2006). A distinct seasonal pattern of the ratio of soil respiration to total ecosystem respiration in a spruce-dominated forest. *Global Change Biology*, *12*(2), 230–239. doi: 10.1111/j.1365-2486.2005.01062.x

Davidson, E. A., Samanta, S., Caramori, S. S., & Savage, K. (2012). The Dual Arrhenius and Michaelis-Menten kinetics model for decomposition of soil organic matter at hourly to seasonal time scales. *Global Change Biology*, *18*(1), 371–384. doi: 10.1111/j.1365-2486.2011.02546.x

Detto, M., Bohrer, G., Nietz, J., Maurer, K., Vogel, C., Gough, C., & Curtis, P. (2013, oct). Multivariate Conditional Granger Causality Analysis for Lagged Response of Soil Respiration in a Temperate Forest. *Entropy*, *15*(12), 4266–4284. Retrieved from http://www.mdpi.com/1099-4300/15/10/4266 doi: 10.3390/e15104266

Diamond, H. J., Karl, T. R., Palecki, M. A., Baker, C. B., Bell, J. E., Leeper, R. D., ... Thorne, P. W. (2013, apr). U.S. Climate Reference Network after One Decade of Operations: Status and Assessment. *Bulletin of the American Meteorological Society*, *94*(4), 485–498. Retrieved from https://journals.ametsoc.org/doi/10.1175/BAMS-D-12-00170.1 doi: 10.1175/BAMS-D-12-00170.1

dos Santos, T., Keppel-Aleks, G., De Roo, R., & Steiner, A. L. (2021). Can Land Surface Models Capture the Observed Soil Moisture Control of Water and Carbon Fluxes in Temperate-To-Boreal Forests? *Journal of Geophysical Research: Biogeosciences*, *126*(4), 1–18. doi: 10.1029/2020jg005999

Endsley, K. A. (2021a). *pyl4c (Version 0.12.0.dev).* Retrieved from https://github.com/arthur-e/pyl4c/ doi: https://doi.org/10.5281/zenodo.5156231

Endsley, K. A. (2021b). *simsoil: Very simple, point-scale soil hydrology model (Version 0.1.0).* Zenodo. doi: http://doi.org/10.5281/zenodo.4906830

Endsley, K. A., Kimball, J. S., Reichle, R. H., & Watts, J. D. (2020, dec). Satellite monitoring of global surface soil organic carbon dynamics using the SMAP Level 4 Carbon Product. *Journal of Geophysical Research: Biogeosciences*, *125*(12). Retrieved from https://onlinelibrary.wiley.com/doi/10.1029/2020JG006100 doi: 10.1029/2020JG006100

Entekhabi, D., Njoku, E. G., O'Neill, P. E., Kellogg, K. H., Crow, W. T., Edelstein, W. N., ... Van Zyl, J. (2010, may). The Soil Moisture Active Passive (SMAP) Mission. *Proceedings of the IEEE*, *98*(5), 704–716. Retrieved from http://ieeexplore.ieee.org/document/5460980/ doi: 10.1109/JPROC.2010.2043918

Forkel, M., Carvalhais, N., Rödenbeck, C., Keeling, R., Heimann, M., Thonicke, K., ... Reichstein, M. (2016). Enhanced seasonal CO2 exchange caused by amplified

plant productivity in northern ecosystems. *Science*, *351*(6274), 696–699. doi: 10.1126/science.aac4971

Forkel, M., Carvalhais, N., Schaphoff, S., Bloh, W. V., Migliavacca, M., Thurner, M., & Thonicke, K. (2014). Identifying environmental controls on vegetation greenness phenology through model-data integration. *Biogeosciences*, *11*(23), 7025–7050. doi: 10.5194/bg-11-7025-2014

Friedl, M. A., Sulla-Menashe, D., Tan, B., Schneider, A., Ramankutty, N., Sibley, A., & Huang, X. (2010, jan). MODIS Collection 5 global land cover: Algorithm refinements and characterization of new datasets. *Remote Sensing of Environment*, *114*(1), 168–182. Retrieved from `https://linkinghub.elsevier.com/retrieve/pii/S0034425709002673` doi: 10.1016/j.rse.2009.08.016

Gaumont-Guay, D., Black, T. A., Barr, A. G., Griffis, T. J., Jassal, R. S., Krishnan, P., ... Nesic, Z. (2014, jan). Eight years of forest-floor CO2 exchange in a boreal black spruce forest: Spatial integration and long-term temporal trends. *Agricultural and Forest Meteorology*, *184*, 25–35. Retrieved from `https://linkinghub.elsevier.com/retrieve/pii/S0168192313002177` doi: 10.1016/j.agrformet.2013.08.010

Gelaro, R., McCarty, W., Suárez, M. J., Todling, R., Molod, A., Takacs, L., ... Zhao, B. (2017, jul). The Modern-Era Retrospective Analysis for Research and Applications, Version 2 (MERRA-2). *Journal of Climate*, *30*(14), 5419–5454. Retrieved from `http://journals.ametsoc.org/doi/10.1175/JCLI-D-16-0758.1` doi: 10.1175/JCLI-D-16-0758.1

Giasson, M. A., Ellison, A. M., Bowden, R. D., Crill, P. M., Davidson, E. A., Drake, J. E., ... Finzi, A. C. (2013). Soil respiration in a northeastern US temperate forest: A 22-year synthesis. *Ecosphere*, *4*(11). doi: 10.1890/ES13.00183.1

Global Soil Data Task Group. (2000). *Global Gridded Surfaces of Selected Soil Characteristics (IGBP-DIS)* (Tech. Rep.). ORNL DAAC. doi: https://doi.org/10.3334/ORNLDAAC/569

Graven, H. D., Keeling, R. F., Piper, S. C., Patra, P. K., Stephens, B. B., Wofsy, S. C., ... Bent, J. D. (2013). Enhanced seasonal exchange of CO2 by Northern ecosystems since 1960. *Science*, *341*(6150), 1085–1089. doi: 10.1126/science.1239207

Hengl, T., De Jesus, J. M., Heuvelink, G. B. M., Gonzalez, M. R., Kilibarda, M., Blagotić, A., ... Kempen, B. (2017). SoilGrids250m: Global gridded soil information based on machine learning. *PLoS ONE*, *12*(2), 1–40. doi: 10.1371/journal.pone.0169748

Heskel, M. A., Atkin, O. K., Turnbull, M. H., & Griffin, K. L. (2013). Bringing the Kok effect to light: A review on the integration of daytime respiration and net ecosystem exchange. *Ecosphere*, *4*(8), 1–14. doi: 10.1890/ES13-00120.1

Hu, Z., Michaletz, S. T., Johnson, D. J., McDowell, N. G., Huang, Z., Zhou, X., & Xu, C. (2018, nov). Traits drive global wood decomposition rates more than climate. *Global Change Biology*, *24*(11), 5259–5269. Retrieved from `http://doi.wiley.com/10.1111/gcb.14357` doi: 10.1111/gcb.14357

Ito, A., Inatomi, M., Huntzinger, D. N., Schwalm, C., Michalak, A. M., Cook, R., ... Zhao, F. (2016). Decadal trends in the seasonal-cycle amplitude of terrestrial CO2 exchange resulting from the ensemble of terrestrial biosphere models. *Tellus, Series B: Chemical and Physical Meteorology*, *68*(1), 1–20. doi: 10.3402/tellusb.v68.28968

Jackson, R. B., Canadell, J., Ehleringer, J. R., Mooney, H. A., Sala, O. E., & Schulze, E. D. (1996). A global analysis of root distributions for terrestrial biomes. *Oecologia*, *108*, 389–411.

Järveoja, J., Nilsson, M. B., Gažovič, M., Crill, P. M., & Peichl, M. (2018). Partitioning of the net CO2 exchange using an automated chamber system reveals plant phenology as key control of production and respiration fluxes in a boreal

peatland. *Global Change Biology*, *24*(8), 3436–3451. doi: 10.1111/gcb.14292

Jassal, R. S., Black, T. A., Novak, M. D., Gaumont-Guay, D., & Nesic, Z. (2008, jun). Effect of soil water stress on soil respiration and its temperature sensitivity in an 18-year-old temperate Douglas-fir stand. *Global Change Biology*, *14*(6), 1305–1318. Retrieved from https://onlinelibrary.wiley.com/doi/10.1111/j.1365-2486.2008.01573.x doi: 10.1111/j.1365-2486.2008.01573.x

Jian, J., Vargas, R., Anderson-Teixeira, K., Stell, E., Herrmann, V., Horn, M., ... Bond-Lamberty, B. (2021). A restructured and updated global soil respiration database (SRDB-V5). *Earth System Science Data*, *13*(2), 255–267. doi: 10.5194/essd-13-255-2021

Johnston, A. S. A., & Sibly, R. M. (2018, oct). The influence of soil communities on the temperature sensitivity of soil respiration. *Nature Ecology & Evolution*, *2*(10), 1597–1602. Retrieved from http://www.nature.com/articles/s41559-018-0648-6 doi: 10.1038/s41559-018-0648-6

Jones, L. A., Kimball, J. S., Reichle, R. H., Madani, N., Glassy, J., Ardizzone, J. V., ... Scott, R. L. (2017). The SMAP Level 4 Carbon Product for Monitoring Ecosystem Land-Atmosphere CO2 Exchange. *IEEE Transactions on Geoscience and Remote Sensing*, *55*(11), 6517–6532. doi: 10.1109/TGRS.2017.2729343

Jung, M., Schwalm, C., Migliavacca, M., Walther, S., Camps-Valls, G., Koirala, S., ... Reichstein, M. (2020). Scaling carbon fluxes from eddy covariance sites to globe: Synthesis and evaluation of the FLUXCOM approach. *Biogeosciences*, *17*(5), 1343–1365. doi: 10.5194/bg-17-1343-2020

Keenan, T. F., Gray, J., Friedl, M. A., Toomey, M., Bohrer, G., Hollinger, D. Y., ... Richardson, A. D. (2014, jul). Net carbon uptake has increased through warming-induced changes in temperate forest phenology. *Nature Climate Change*, *4*(7), 598–604. Retrieved from http://www.nature.com/articles/nclimate2253 doi: 10.1038/nclimate2253

Keenan, T. F., Migliavacca, M., Papale, D., Baldocchi, D., Reichstein, M., Torn, M., & Wutzler, T. (2019). Widespread inhibition of daytime ecosystem respiration. *Nature Ecology and Evolution*, *3*(3), 407–415. Retrieved from http://dx.doi.org/10.1038/s41559-019-0809-2 doi: 10.1038/s41559-019-0809-2

Kimball, J. S., Jones, L. A., Zhang, K., Heinsch, F. A., McDonald, K. C., & Oechel, W. C. (2009). A satellite approach to estimate land-atmosphere CO2 exchange for boreal and Arctic biomes using MODIS and AMSR-E. *IEEE Transactions on Geoscience and Remote Sensing*, *47*(2), 569–587. doi: 10.1109/TGRS.2008.2003248

Koster, R. D., Guo, Z., Yang, R., Dirmeyer, P. A., Mitchell, K., & Puma, M. J. (2009, aug). On the nature of soil moisture in land surface models. *Journal of Climate*, *22*(16), 4322–4335. Retrieved from http://journals.ametsoc.org/doi/abs/10.1175/2009JCLI2832.1 doi: 10.1175/2009JCLI2832.1

Koster, R. D., Suarez, M. J., Ducharne, A., Stieglitz, M., & Kumar, P. (2000, oct). A catchment-based approach to modeling land surface processes in a general circulation model: 1. Model structure. *Journal of Geophysical Research: Atmospheres*, *105*(D20), 24809–24822. Retrieved from http://doi.wiley.com/10.1029/2000JD900328http://doi.wiley.com/10.1029/2000JD900327 doi: 10.1029/2000JD900327

Koven, C. D., Hugelius, G., Lawrence, D. M., & Wieder, W. R. (2017, nov). Higher climatological temperature sensitivity of soil carbon in cold than warm climates. *Nature Climate Change*, *7*(11), 817–822. Retrieved from http://www.nature.com/articles/nclimate3421 doi: 10.1038/nclimate3421

Koven, C. D., Riley, W. J., Subin, Z. M., Tang, J. Y., Torn, M. S., Collins, W. D., ... Swenson, S. C. (2013). The effect of vertically resolved soil biogeochemistry and alternate soil C and N models on C dynamics of CLM4. *Biogeosciences*, *10*(11), 7109–7131. doi: 10.5194/bg-10-7109-2013

Lawrence, D. M., Fisher, R. A., Koven, C. D., Oleson, K. W., Swenson, S. C., Bonan, G. B., ... (2019, dec). The Community Land Model version 5: Description of new features, benchmarking, and impact of forcing uncertainty. *Journal of Advances in Modeling Earth Systems*, *11*(12), 4245–4287. Retrieved from https://onlinelibrary.wiley.com/doi/abs/10.1029/2018MS001583 doi: 10.1029/2018MS001583

Leitner, S., Sae-Tun, O., Kranzinger, L., Zechmeister-Boltenstern, S., & Zimmermann, M. (2016, jun). Contribution of litter layer to soil greenhouse gas emissions in a temperate beech forest. *Plant and Soil*, *403*(1-2), 455–469. Retrieved from http://link.springer.com/10.1007/s11104-015-2771-3 doi: 10.1007/s11104-015-2771-3

Messerschmidt, J., Parazoo, N. C., Wunch, D., Deutscher, N. M., Roehl, C., Warneke, T., & Wennberg, P. O. (2013). Evaluation of seasonal atmosphere-biosphere exchange estimations with TCCON measurements. *Atmospheric Chemistry and Physics*, *13*(10), 5103–5115. doi: 10.5194/acp-13-5103-2013

Migliavacca, M., Reichstein, M., Richardson, A. D., Mahecha, M. D., Cremonese, E., Delpierre, N., ... Cescatti, A. (2015). Influence of physiological phenology on the seasonal pattern of ecosystem respiration in deciduous forests. *Global Change Biology*, *21*(1), 363–376. doi: 10.1111/gcb.12671

Myneni, R. B., Knyazikhin, Y., & Park, T. (2015). *MCD15A2H MODIS/Terra+Aqua Leaf Area Index/FPAR 8-day L4 Global 500m SIN Grid V006 [Data set].* Retrieved 2021-07-02, from https://doi.org/10.5067/MODIS/MCD15A2H.006 doi: https://doi.org/10.5067/MODIS/MCD15A2H.006

Nielsen, T. F., Ravn, N. R., & Michelsen, A. (2019, nov). Increased CO2 efflux due to long-term experimental summer warming and litter input in subarctic tundra – CO2 fluxes at snowmelt, in growing season, fall and winter. *Plant and Soil*, *444*(1-2), 365–382. Retrieved from http://link.springer.com/10.1007/s11104-019-04282-9 doi: 10.1007/s11104-019-04282-9

Noormets, A., Chen, J., Gu, L., & Desai, A. (2009). The phenology of gross ecosystem productivity and ecosystem respiration in temperate hardwood and conifer chronosequences. *Phenology of Ecosystem Processes: Applications in Global Change Research*, 1–275. doi: 10.1007/978-1-4419-0026-5

Noormets, A., Gavazzi, M. J., Mcnulty, S. G., Domec, J.-C., Sun, G., King, J. S., & Chen, J. (2010, jan). Response of carbon fluxes to drought in a coastal plain loblolly pine forest. *Global Change Biology*, *16*(1), 272–287. Retrieved from https://onlinelibrary.wiley.com/doi/10.1111/j.1365-2486.2009.01928.x doi: 10.1111/j.1365-2486.2009.01928.x

Oikawa, P. Y., Grantz, D. A., Chatterjee, A., Eberwein, J. E., Allsman, L. A., & Jenerette, G. D. (2014, apr). Unifying soil respiration pulses, inhibition, and temperature hysteresis through dynamics of labile soil carbon and O2. *Journal of Geophysical Research: Biogeosciences*, *119*(4), 521–536. Retrieved from http://doi.wiley.com/10.1002/2013JG002434 doi: 10.1002/2013JG002434

Papale, D., & Valentini, R. (2003). A new assessment of European forests carbon exchanges by eddy fluxes and artificial neural network spatialization. *Global Change Biology*, *9*(4), 525–535. doi: 10.1046/j.1365-2486.2003.00609.x

Parazoo, N. C., Arneth, A., Pugh, T. A. M., Smith, B., Steiner, N., Luus, K., ... Miller, C. (2018). Spring photosynthetic onset and net CO2 uptake in Alaska triggered by landscape thawing. *Global Change Biology*, *24*(8), 3416–3435. doi: 10.1111/gcb.14283

Peng, S., Ciais, P., Chevallier, F., Peylin, P., Cadule, P., Sitch, S., ... Wang, X. (2014). Global biogeochemical cycles simulated by terrestrial ecosystem models. *Global Biogeochemical Cycles*, *29*, 46–64. doi: 10.1002/2014GB004931.Received

Peng, S., Ciais, P., Chevallier, F., Peylin, P., Cadule, P., Sitch, S., ... Zhao, H. (2015, jan). Benchmarking the seasonal cycle of CO2 fluxes simulated

by terrestrial ecosystem models. *Global Biogeochemical Cycles*, *29*(1), 46–64. Retrieved from http://doi.wiley.com/10.1002/2014GB004931 doi: 10.1002/2014GB004931

Peng, S., Piao, S., Ciais, P., Myneni, R. B., Chen, A., Chevallier, F., ... Zeng, H. (2013). Asymmetric effects of daytime and night-time warming on Northern Hemisphere vegetation. *Nature*, *501*(7465), 88–92. doi: 10.1038/nature12434

Randerson, J. T., Thompson, M. V., Malmstrom, C. M., Field, C. B., & Fung, I. Y. (1996). Substrate limitations for heterotrophs: Implications for models that estimate the seasonal cycle of atmospheric CO2. *Global Biogeochemical Cycles*, *10*(4), 585–602. doi: 10.1029/96GB01981

Reichle, R. H., De Lannoy, G., Koster, R. D., Crow, W. T., Kimball, J. S., & Liu, Q. (2019). *SMAP L4 Global 3-hourly 9 km EASE-Grid Surface and Root Zone Soil Moisture Geophysical Data, Version 4.* Boulder, Colorado, U.S.A.: NASA National Snow and Ice Data Center Distributed Active Archive Center. Retrieved 2019-08-01, from https://nsidc.org/data/SPL4SMGP doi: 10.5067/KPJNN2GI1DQR

Reichle, R. H., De Lannoy, G. J. M., Liu, Q., Koster, R. D., Kimball, J. S., Crow, W. T., ... Smith, E. B. (2017, dec). Global Assessment of the SMAP Level-4 Surface and Root-Zone Soil Moisture Product Using Assimilation Diagnostics. *Journal of Hydrometeorology*, *18*(12), 3217–3237. Retrieved from http://journals.ametsoc.org/doi/10.1175/JHM-D-17-0130.1 doi: 10.1175/JHM-D-17-0130.1

Reichstein, M., Rey, A., Freibauer, A., Tenhunen, J., Valentini, R., Banza, J., ... Yakir, D. (2003). Modeling temporal and large-scale spatial variability of soil respiration from soil water availability, temperature and vegetation productivity indices. *Global Biogeochemical Cycles*, *17*(4). doi: 10.1029/2003gb002035

Richardson, A. D., Andy Black, T., Ciais, P., Delbart, N., Friedl, M. A., Gobron, N., ... Varlagin, A. (2010, oct). Influence of spring and autumn phenological transitions on forest ecosystem productivity. *Philosophical Transactions of the Royal Society B: Biological Sciences*, *365*(1555), 3227–3246. Retrieved from https://royalsocietypublishing.org/doi/10.1098/rstb.2010.0102 doi: 10.1098/rstb.2010.0102

Ryan, E. M., Ogle, K., Zelikova, T. J., Lecain, D. R., Williams, D. G., Morgan, J. A., & Pendall, E. (2015). Antecedent moisture and temperature conditions modulate the response of ecosystem respiration to elevated CO2 and warming. *Global Change Biology*, *21*(7), 2588–2602. doi: 10.1111/gcb.12910

Sánchez-Cañete, E. P., Oyonarte, C., Serrano-Ortiz, P., Curiel Yuste, J., Pérez-Priego, O., Domingo, F., & Kowalski, A. S. (2016, aug). Winds induce CO2 exchange with the atmosphere and vadose zone transport in a karstic ecosystem. *Journal of Geophysical Research: Biogeosciences*, *121*(8), 2049–2063. Retrieved from http://doi.wiley.com/10.1002/2016JG003500 doi: 10.1002/2016JG003500

Schaefer, G. L., Cosh, M. H., & Jackson, T. J. (2007, dec). The USDA Natural Resources Conservation Service Soil Climate Analysis Network (SCAN). *Journal of Atmospheric and Oceanic Technology*, *24*(12), 2073–2077. Retrieved from http://journals.ametsoc.org/doi/10.1175/2007JTECHA930.1 doi: 10.1175/2007JTECHA930.1

Shi, M., Parazoo, N. C., Jeong, S. J., Birch, L., Lawrence, P., Euskirchen, E. S., & Miller, C. E. (2020). Exposure to cold temperature affects the spring phenology of Alaskan deciduous vegetation types. *Environmental Research Letters*, *15*(2). doi: 10.1088/1748-9326/ab6502

Sihi, D., Davidson, E. A., Chen, M., Savage, K. E., Richardson, A. D., Keenan, T. F., & Hollinger, D. Y. (2018). Merging a mechanistic enzymatic model of soil heterotrophic respiration into an ecosystem model in two AmeriFlux sites of

northeastern USA. *Agricultural and Forest Meteorology*, *252*(May 2017), 155–166. Retrieved from https://doi.org/10.1016/j.agrformet.2018.01.026 doi: 10.1016/j.agrformet.2018.01.026

Sulman, B. N., Desai, A. R., Schroeder, N. M., Ricciuto, D., Barr, A., Richardson, A. D., ... Weng, E. (2012). Impact of hydrological variations on modeling of peatland CO2 fluxes: Results from the North American Carbon Program site synthesis. *Journal of Geophysical Research: Biogeosciences*, *117*(1), 1–21. doi: 10.1029/2011JG001862

Tao, J., Reichle, R. H., Koster, R. D., Forman, B. A., & Xue, Y. (2017). Evaluation and Enhancement of Permafrost Modeling With the NASA Catchment Land Surface Model. *Journal of Advances in Modeling Earth Systems*, *9*(7), 2771–2795. doi: 10.1002/2017MS001019

Thum, T., Nabel, J. E. M. S., Tsuruta, A., Aalto, T., Dlugokencky, E. J., Liski, J., ... Zaehle, S. (2020, nov). Evaluating two soil carbon models within the global land surface model JSBACH using surface and spaceborne observations of atmospheric CO2. *Biogeosciences*, *17*(22), 5721–5743. Retrieved from https://bg.copernicus.org/articles/17/5721/2020/ doi: 10.5194/bg-17-5721-2020

Turner, D. P., Ritts, W. D., Cohen, W. B., Gower, S. T., Running, S. W., Zhao, M., ... Ahl, D. E. (2006, jun). Evaluation of MODIS NPP and GPP products across multiple biomes. *Remote Sensing of Environment*, *102*(3-4), 282–292. Retrieved from https://linkinghub.elsevier.com/retrieve/pii/S0034425706000873 doi: 10.1016/j.rse.2006.02.017

Ueyama, M., Yoshikawa, K., & Takagi, K. (2018, jul). A cool-temperate young larch plantation as a net methane source - A 4-year continuous hyperbolic relaxed eddy accumulation and chamber measurements. *Atmospheric Environment*, *184*, 110–120. Retrieved from https://linkinghub.elsevier.com/retrieve/pii/S1352231018302565 doi: 10.1016/j.atmosenv.2018.04.025

Vargas, R., Sánchez-Cañete P, E., Serrano-Ortiz, P., Curiel Yuste, J., Domingo, F., López-Ballesteros, A., & Oyonarte, C. (2018, aug). Hot-Moments of Soil CO2 Efflux in a Water-Limited Grassland. *Soil Systems*, *2*(3), 47. Retrieved from http://www.mdpi.com/2571-8789/2/3/47 doi: 10.3390/soilsystems2030047

Wan, J., Tokunaga, T. K., Dong, W., Williams, K. H., Kim, Y., Conrad, M. E., ... Hubbard, S. S. (2018, sep). Deep Unsaturated Zone Contributions to Carbon Cycling in Semiarid Environments. *Journal of Geophysical Research: Biogeosciences*, *123*(9), 3045–3054. Retrieved from https://onlinelibrary.wiley.com/doi/10.1029/2018JG004669 doi: 10.1029/2018JG004669

Watts, J. D., Kimball, J. S., Parmentier, F. J. W., Sachs, T., Rinne, J., Zona, D., ... Aurela, M. (2014, apr). A satellite data driven biophysical modeling approach for estimating northern peatland and tundra CO₂ and CH₄ fluxes. *Biogeosciences*, *11*(7), 1961–1980. Retrieved from https://bg.copernicus.org/articles/11/1961/2014/ doi: 10.5194/bg-11-1961-2014

Wehr, R., Munger, J. W., McManus, J. B., Nelson, D. D., Zahniser, M. S., Davidson, E. A., ... Saleska, S. R. (2016). Seasonality of temperate forest photosynthesis and daytime respiration. *Nature*, *534*(7609), 680–683. Retrieved from http://dx.doi.org/10.1038/nature17966 doi: 10.1038/nature17966

Winnick, M. J., Lawrence, C. R., McCormick, M., Druhan, J. L., & Maher, K. (2020). Soil respiration response to rainfall modulated by plant phenology in a montane meadow, East River, Colorado, USA. *Journal of Geophysical Research: Biogeosciences*, *125*(10), 1–20. doi: 10.1029/2020JG005924

Wohlfahrt, G., Bahn, M., Haslwanter, A., Newesely, C., & Cernusca, A. (2005). Estimation of daytime ecosystem respiration to determine gross primary production of a mountain meadow. *Agricultural and Forest Meteorology*, *130*(1-2), 13–25. doi:

10.1016/j.agrformet.2005.02.001

Wu, C., Chen, J. M., Black, T. A., Price, D. T., Kurz, W. A., Desai, A. R., ... Blanken, P. D. (2013). Interannual variability of net ecosystem productivity in forests is explained by carbon flux phenology in autumn. *Global Ecology and Biogeography*, *22*(8), 994–1006. doi: 10.1111/geb.12044

Yi, Y., Kimball, J. S., Jones, L. A., Reichle, R. H., Nemani, R., & Margolis, H. A. (2013, jun). Recent climate and fire disturbance impacts on boreal and arctic ecosystem productivity estimated using a satellite-based terrestrial carbon flux model. *Journal of Geophysical Research: Biogeosciences*, *118*(2), 606–622. Retrieved from `http://doi.wiley.com/10.1002/jgrg.20053` doi: 10.1002/jgrg.20053

Yi, Y., Kimball, J. S., Watts, J. D., Natali, S. M., Zona, D., Liu, J., ... Miller, C. E. (2020, nov). Investigating the sensitivity of soil heterotrophic respiration to recent snow cover changes in Alaska using a satellite-based permafrost carbon model. *Biogeosciences*, *17*(22), 5861–5882. Retrieved from `https://bg.copernicus.org/articles/17/5861/2020/` doi: 10.5194/bg-17-5861-2020

Zhang, Q., Phillips, R. P., Manzoni, S., Scott, R. L., Oishi, A. C., Finzi, A., ... Novick, K. A. (2018, sep). Changes in photosynthesis and soil moisture drive the seasonal soil respiration-temperature hysteresis relationship. *Agricultural and Forest Meteorology*, *259*, 184–195. Retrieved from `https://linkinghub.elsevier.com/retrieve/pii/S0168192318301515` doi: 10.1016/j.agrformet.2018.05.005

Zhao, F., & Zeng, N. (2014, dec). Continued increase in atmospheric CO2 seasonal amplitude in the 21st century projected by the CMIP5 Earth system models. *Earth System Dynamics*, *5*(2), 423–439. Retrieved from `https://esd.copernicus.org/articles/5/423/2014/` doi: 10.5194/esd-5-423-2014

Zhao, F., Zeng, N., Asrar, G., Friedlingstein, P., Ito, A., Jain, A., ... Zaehle, S. (2016). Role of CO2, climate and land use in regulating the seasonal amplitude increase of carbon fluxes in terrestrial ecosystems: A multimodel analysis. *Biogeosciences*, *13*(17), 5121–5137. doi: 10.5194/bg-13-5121-2016

Ťupek, B., Launiainen, S., Peltoniemi, M., Sievänen, R., Perttunen, J., Kulmala, L., ... Lehtonen, A. (2019). Evaluating CENTURY and Yasso soil carbon models for CO2 emissions and organic carbon stocks of boreal forest soil with Bayesian multi-model inference. *European Journal of Soil Science*, *70*(4), 847–858. doi: 10.1111/ejss.12805